ANTIOXIDANTS & REDOX SIGNALING
Volume 13, Number 8, 2010

DOI: 10.1089/ars.2010.3109

COMPREHENSIVE INVITED REVIEW

Conformational Plasticity and Structure/Function Relationships in Cytochromes P450

Thomas C. Pochapsky,[1–3] Sophia Kazanis,[1] and Marina Dang[1]

Abstract

The cytochrome P450s are a superfamily of enzymes that are found in all kingdoms of living organisms, and typically catalyze the oxidative addition of atomic oxygen to an unactivated C-C or C-H bond. Over 8000 nonredundant sequences of putative and confirmed P450 enzymes have been identified, but three-dimensional structures have been determined for only a small fraction of these. While all P450 enzymes for which structures have been determined share a common global fold, the flexibility and modularity of structure around the active site account for the ability of P450 enzymes to accommodate a vast number of structurally dissimilar substrates and support a wide range of selective oxidations. In this review, known P450 structures are compared, and some structural criteria for prediction of substrate selectivity and reaction type are suggested. The importance of dynamic processes such as redox-dependent and effector-induced conformational changes in determining catalytic competence and regio- and stereoselectivity is discussed, and noncrystallographic methods for characterizing P450 structures and dynamics, in particular, mass spectrometry and nuclear magnetic resonance spectroscopy are reviewed. *Antioxid. Redox Signal.* 13, 1273–1296.

I. Introduction

IT IS NOW OVER 50 YEARS since the tertiary structure of a protein was first established by X-ray crystallography (50), and 45 years have passed since the first enzyme structure, that of hen egg lysozyme, was described (9). A trickle of protein structures in the 1970s has turned into a flood: 65 unique structures (<90% sequence identity) were added to the PDB database between 1970 and 1980, whereas over 2300 structures were released in the first 9 months of 2009 alone. The

Reviewing Editors: *Sean C. Gay, Gideon Grogan, David Leys, Kirsty McLean, and Mark A. White*

Departments of [1]Chemistry and [2]Biochemistry, and [3]the Rosenstiel Basic Medical Science Research Institute, Brandeis University, Waltham, Massachusetts.

importance of structure determination to our understanding of enzyme function cannot be overstated: active sites are readily identified, critical residues are often obvious, and catalytic mechanisms can be proposed and tested based on the information that these structures provide. Yet a crystallographically-determined enzyme structure is not a panacea. Often, a newly determined enzyme structure raises more questions than it answers. Why does the substrate (or substrate analog) seem to be in the wrong orientation for the observed chemistry? Are we seeing all of the binding sites, or are there secondary (allosteric) sites that are unoccupied? Is the structure that we see biologically relevant? Sometimes the answers to these questions are obvious, but not always. For example, crystal packing can force order upon regions of the polypeptide that in solution have multiple functionally important conformations. It can also select for a single conformation in regions where conformational changes are critical to the enzyme activity. It is therefore important to keep in mind that a crystallographic enzyme structure presents a snapshot of a dynamic system. It is not always easy to tell where on a reaction pathway the observed conformation of an enzyme lies, or even if the observed conformer is functionally important.

Nowhere are these considerations more important than when thinking about structure/function relationships in cytochromes P450. The P450 enzymes are heme-containing monooxygenases that catalyze the oxidation of organic species by molecular oxygen, often by insertion of an oxygen atom into an unactivated C-H or C-C bond. Members of the P450 superfamily are found in every kingdom and phylum of living organism, from archaea to chordates. They catalyze a wide variety of oxidative transformations that are essential to primary and secondary metabolic processes. In humans, P450 enzymes play important roles in drug metabolism and activation, carcinogen activation, steroid and prostaglandin biosyntheses, and as such provide a wide variety of therapeutic targets (77). In other organisms, P450s are critical for the biosynthesis of antibiotics and antineoplastics, and are the focus of research aimed at tailoring and modifying their activity so as to produce novel pharmaceuticals.

While most bacterial and archaeal P450s are water-soluble monomeric enzymes, P450s found in higher organisms are usually membrane-bound or membrane-associated, and present considerable challenges to the structural biologist. An additional factor that must be considered when examining the structures of redox-active enzymes such as P450s is that both structure and dynamics can be affected by the oxidation state of the redox-active functionality (heme, in the case of P450) (73, 98). Unless precautions are taken, reduction of metal centers by photoelectrons produced by the incident X-ray beam can render the oxidation state of the redox-active center ambiguous in crystallographically-derived structures.

In the past, P450 enzymes were often classified according to the type of electron transfer protein that supplies the reducing equivalents required for turnover. For example, many P450s are reduced directly by NAD(P)H-dependent flavoproteins, whereas others use ferredoxins as intermediate electron shuttles. However, it has become evident that the electron transport chains supporting P450-catalyzed oxidations are often more complicated than previously suspected (36), and that electron transfer partners often serve dual roles, functioning as effectors as well as reducing agents (70, 169).

As will be seen in this review, the P450 superfamily combines a conservative architecture with a remarkable adaptability for substrate recognition and regio- and stereoselectivity in the chemistry that is catalyzed. This is possible due to the modular nature of secondary structural features surrounding the P450 active site. Not only do these features differ between enzymes, but they change even between different states of the individual enzyme. In this review, we have chosen examples that we hope will demonstrate this modularity, while attempting to find common themes, where possible, in comparing P450 structures. Nevertheless, it is becoming clear that P450 enzyme structures must be considered, not just in three dimensions, but in four, as flexible and dynamic arrangements that change depending upon the presence of substrate, cofactor, and oxidation state.

II. Crystallographic Structures of Prokaryotic Cytochromes P450

A. CYP101

The first crystallographic structures of P450 were determined for a soluble monomeric bacterial enzyme, cytochrome $P450_{cam}$ (CYP101) a camphor hydroxylase from the soil bacterium *Pseudomonas putida* (108–110, 113–118). Being a bacterial enzyme, CYP101 is relatively easy to express, handle, and purify, and much of what we currently know or suspect about the P450 enzyme superfamily has been learned using this enzyme. The CYP101 structure is a roughly triangular prism, with secondary structural features being conveniently described in terms of their location relative to the plane of the heme porphyrin macrocycle. As in all P450s, the heme iron is axially ligated by a cysteine thiolate that defines the *proximal* side of the heme. The active site is on the opposite (*distal*) face of the heme, and, depending upon the oxidation state of the enzyme, the distal Fe axial ligand might be O_2, water, hydroxide, or other Lewis base. In the presence of substrate, the distal axial ligation site can be vacant, yielding the 5-coordinate geometry expected for high-spin Fe (III). The secondary structure nomenclature scheme initially adopted by Poulos *et al.* for CYP101 (109) has become standard for describing secondary structural features in all P450s, and is summarized in Figures 1 and 2. Viewed from the distal side of the protein in the orientation shown in Figure 1, the active site of CYP101 is bound to the "north" by helix I, to the "west" by the B′ helix and B′–C loop, "south" by residues of the β3 sheet, and "east" by the β5 sheet. The floor of the active site is provided by the heme porphyrin, while the active site is effectively closed off from solvent by a cap formed by the F and G helices and the F-G loop. The orientation of substrate in the CYP101 active site readily explains both the regio- and stereoselectivity of the observed hydroxylation at the 5-*exo* position of camphor.

Viewed from the north as defined in Figure 1, proximal features that can be seen in Figure 2 include the B, C, J, K, and L helices, as well as a region of irregular structure preceding the axial ligand Cys known as the "β-meander", the β2 and portions of the β4 sheets. The D helix is approximately bisected by the plane of the heme. On the distal side, the I helix is the most prominent structural feature, providing a backbone around which the heme and the remainder of the polypeptide are arranged. As in almost all P450 structures, the I helix in CYP101 is not completely straight, but is "kinked" near the heme iron due to an interruption in the regular $i, i+4$ NH—O=C hydrogen bonding pattern of a regular α-helix. This interruption is due to a hydrogen bond from the OH of a

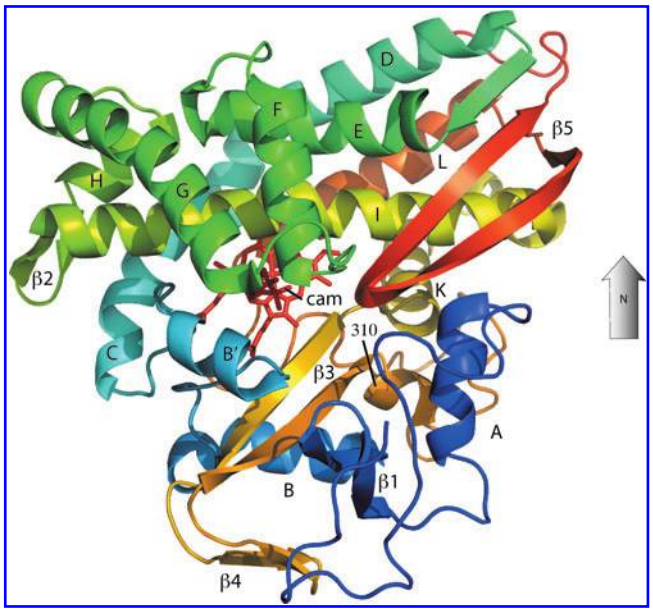

FIG. 1. Structure of camphor hydroxylase CYP101 (cytochrome $P450_{cam}$) from PDB entry 2CPP, as viewed from the distal face. Secondary structural features are labeled according to the scheme of Poulos (109). Secondary structural features are color-coded from N-terminal (*blue*) to C-terminal (*red*). The *directional arrow* marked "N" indicates the "north" described in the text. (For interpretation of the references to color in this figure legend, the reader is referred to the web version of this article at www.liebertonline.com/ars). Except where noted, all figures were generated using PyMOL (20). (For interpretation of the references to color in this figure legend, the reader is referred to the web version of this article at www.liebertonline.com/ars).

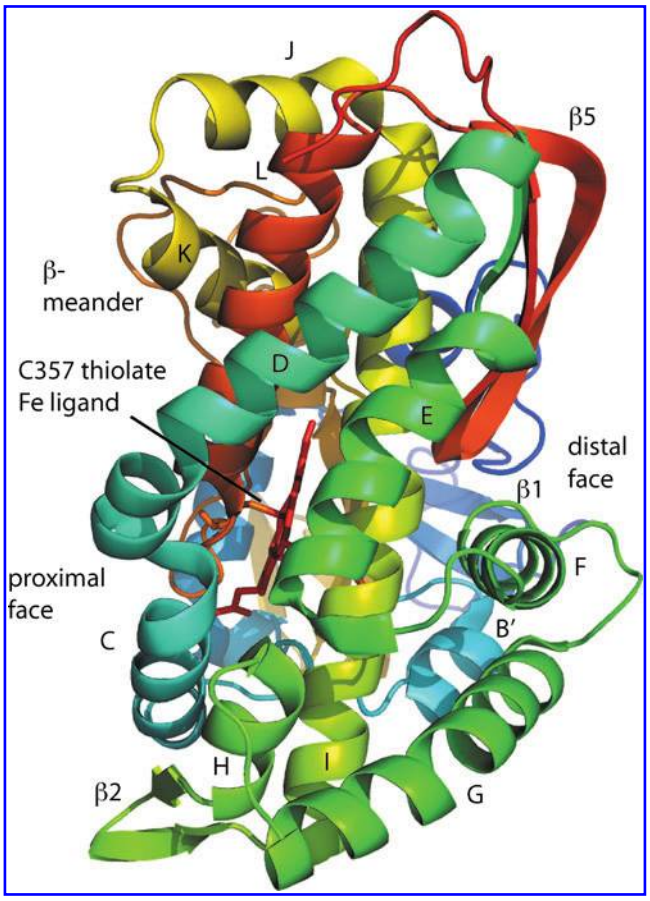

FIG. 2. Structure of CYP101 (cytochrome $P450_{cam}$) from PDB entry 2CPP, as viewed from the "north" face (top of structure in Fig. 1). Distal and proximal features refer to position with respect to the plane of the heme. Secondary structural features are color-coded from N-terminal (*blue*) to C-terminal (*red*). (For interpretation of the references to color in this figure legend, the reader is referred to the web version of this article at www.liebertonline.com/ars).

strongly conserved threonine (Thr 252 in CYP101) to the carbonyl of the *i*-4 residue (Gly 238), and has been proposed to accommodate the bound dioxygen appropriately for the observed chemistry (107). Most of the regular β-sheet structures of CYP101 are located on the distal side, as are the A, B′, E, F, G, and H helices. An additional short region of 3–10 helix is also present on the distal side, providing the apex of a rough pyramidal arrangement of helices A, B and K.

B. CYP102 and CYP108

For some years (1986–1993), the CYP101 structure was the only P450 structure available, and so was used extensively for modeling other P450 enzymes (3, 13, 32, 42, 46, 106, 179). There was initially concern about the validity of such models in the absence of other experimentally determined P450 structures, as the CYP101 fold was unique among known globular protein structures, and sequence homology between CYP101 and most eukaryotic P450s is low (106). However, the structure determination of the heme-binding domain of cytochrome $P450_{BM3}$ (CYP102) (Fig. 3), a fatty acid ω-2-hydroxylase from *Bacillus megaterium*, showed that the P450 fold is indeed conserved (119). Despite low overall sequence homology between the two enzymes (16% sequence identity), it was found that both enzymes have identical topology and that most of the secondary structural features of CYP102 have homologues in CYP101. For convenience, in the course of this review, we will use the CYP101 nomenclature to identify homologous sequence/structural motifs in other P450s, even if the secondary structure is not identical: that is, regions sequentially and structurally homologous with the β5 sheet in CYP101 will be identified as β5, although this region is not a well-defined β-sheet in many P450 structures.

The CYP102 structure provided the first indications of the plasticity of the P450 substrate binding regions. The published CYP101 structures showed relatively modest differences in active site structure, depending on the absence or presence or type of substrate. The most prominent differences observed in the active site were the number of water molecules present and their mobility (109, 110, 115–118). Even with a bulky inhibitor bound, the primary changes observed were to the orientations of side chains near the substrate binding site (113). On the other hand, the original CYP102 asymmetric unit contained two molecules, with one substrate binding site being considerably more open than the other (119). Not surprisingly, the contributions from side chains of residues 14–47, the β1, β3, and β5 sheets, as well as the B′ and F helices makes the substrate binding domain of CYP102 more extensive than that of CYP101. The resulting 22 Å hydrophobic channel resembles the binding domains of

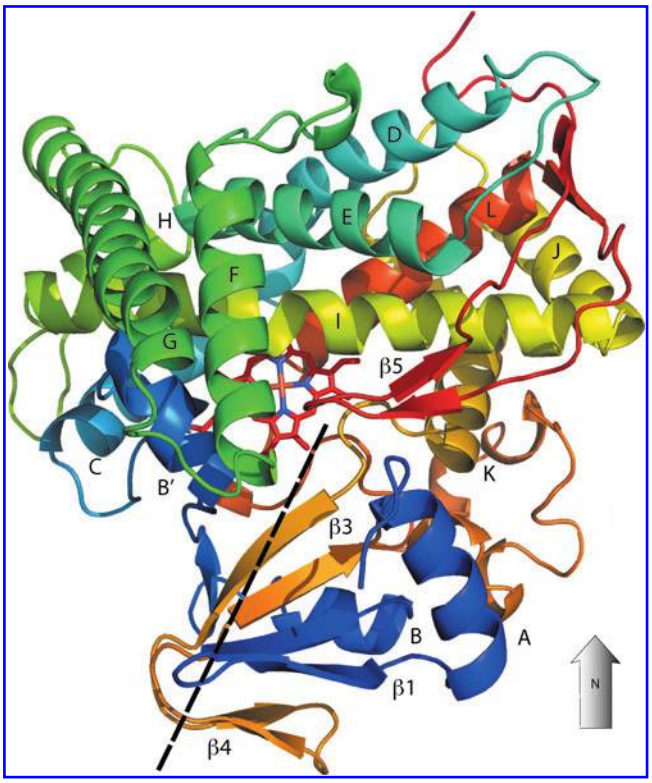

FIG. 3. Structure of fatty acid ω-2 hydroxylase CYP102 (cytochrome $P450_{BM3}$) from PDB entry 1BVY (133), as viewed from the distal face. Secondary structural features are labeled in analogy to structure of CYP101 (Fig. 1). Secondary structural features are color-coded from N-terminal (*blue*) to C-terminal (*red*). Approximate position of the substrate binding channel as reported by Ravichandran *et al.* is indicated by a *dotted line* (119). (For interpretation of the references to color in this figure legend, the reader is referred to the web version of this article at www.liebertonline.com/ars).

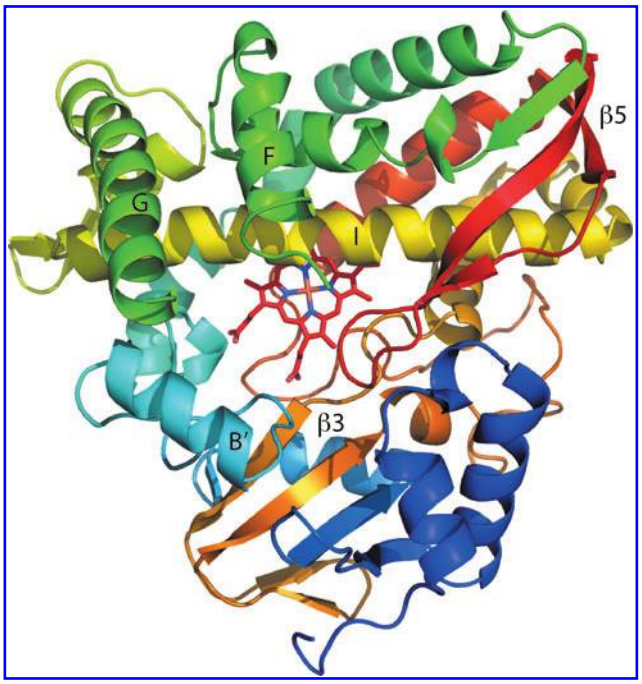

FIG. 4. CYP108 (cytochrome P450terp), from PDB entry 1CPT (37), viewed from distal face in the same orientation as Figures 1 and 3 (see *directional arrow*). Note the absence of the F–G loop, which is disordered in the crystal. (For interpretation of the references to color in this figure legend, the reader is referred to the web version of this article at www.liebertonline.com/ars).

other enzymes that interact with fatty acids and long-chain lipophilic molecules. Comparison of the two molecules in the original CYP102 asymmetric unit shows significant displacements (rms deviations of 1.8 Å) of residues 1–49, the B′ helix, the F–G loop, and portions of the β5 sheet; in short, residues involved in substrate binding and orientation (119).

The structure of CYP108 ($P450_{terp}$), another bacterial enzyme from *Pseudomonas*, also showed remarkable variability in the substrate binding region. The structure was solved in the absence of substrate (α-terpineol), and the F–G loop expected to cap the active site was disordered in the crystal. This disorder leaves the active site essentially exposed to solvent in the crystal (Fig. 4). In addition, the B′ helix that abuts the active site in CYP101 is significantly farther from the heme in CYP108. While the N-terminal of the B′ helix in CYP101 is slightly farther from the Fe atom in CYP101 than CYP108 (20.5 Å vs. 19.0 Å), the midpoint of the B′ helix is almost 7 Å farther from the Fe atom in CYP108 than in CYP101. In spite of this, characterization of heme that was covalently modified by phenylhydrazine in the CYP108 active site suggests that it is more restricted than the active sites of either CYP101 or CYP102 (27). Clearly, a significant conformational change is required in CYP108 in order to accomplish this restriction.

C. Macrolide biosynthetic P450s

Another early focus of P450 structural biology was the class of enzymes involved in macrocyclic antibiotic biosynthesis by oxidative modification. These enzymes are of obvious interest for their potential in bioengineering of novel antibiotics, and structures for a number of enzymes of this type have been characterized. CYP107 (P450 EryF) from *Saccharopolyspora erythreae* stereospecifically hydroxylates the macrolide ring in one step of erythromycin biosynthesis, and was the first structure in this class to be determined (18). This structure was obtained with a macrolide (6-deoxyerythronolide B) bound, and the B′ helix adjacent to the substrate binding site is segmented, with a small helical region preceding the B′ helix, the long axis of which is, as in CYP108, tilted away from the active site, increasing the size of the active site relative to that of CYP101. This is not particularly surprising, given that the macrolide substrate is considerably larger in CYP107 than camphor in CYP101. Also, the F and G helices are both longer than in CYP101 by a single helical turn, making the F–G loop relatively short, and likely less flexible than that in CYP101. The macrolide carbon that is hydroxylated is located close to the heme iron (4.6 Å), but so is a substrate methyl group that is not oxidized. As such, it is unclear whether further rearrangement of the enzyme–substrate complex is necessary in order to reach the correct conformation for the observed chemistry.

A related series of structures, those for CYP113A1 (EryK), which catalyzes the 12-hydroxylation of erythromycin D in *S. erythreae*, have recently been published (127). This hydroxylation is the penultimate step in erythromycin A

biosynthesis, and the substrate differs from that of CYP107 in that the macrolide is substituted with two sugar moieties, and as such is considerably larger than the macrolide substrate for CYP107. The sequences of CYP113A1 and CYP107 are fairly similar (34% identity). However, the B′ helix of CYP107 is absent in CYP113A1, and is replaced by a short turn-loop-turn motif joining the B and C helices. On the other hand, the F–G loop (short in CYP107) is longer in CYP113A1, and the sugar moieties of the substrate interact primarily with the F–G loop and G helix. The structures of CYP113A1 with and without substrate bound show considerable differences in the positions of both the B–C and F–G loops, indicating that rearrangement of these loops are an integral part of substrate binding. Interestingly, recently described structures for CYP107L1 (PikC) (66, 135) from *Streptomyces venezuelae* appear to combine features of both CYP107 and CYP113A1: a short F–G loop (as in CYP107) and relatively complex turn-loop arrangement bridging the B and C helices (as in CYP113A1). This enzyme is broader spectrum, productively binding a number of different desosaminosugar-substituted macrolides. Li and coworkers have parlayed the presence of a desosamine binding site in PikC into an interesting approach for producing novel oxidations by introducing the desosamine group into potential substrates. The desosamine group binding site in PikC is fixed with contacts on the β3 and β5 (south and east) edges of the active site. The position of oxidation of the attached substrate is then determined by where the desosamine is attached (66, 67).

Another variation on the theme of macrolide biosynthetic P450s is found with P450 EpoK, from the myxobacterium *Sorangium cellulosum*, which catalyzes the epoxidation of epothilone C and D to epothilone A and B, respectively. These compounds are under investigation as potential antineoplastics. Unlike the antibiotic macrolides, these compounds are substituted with a pendant thiazole moiety instead of sugars or desosamino sugars. In the structures of Nagano *et al*. (87), the thiazole interacts with residues on the F and I helices, as well as residues in the B–C turn loops. Unlike other P450 structures characterized to date, the F and G helices are crossed in these structures, with the long F–G loop allowing the G helix to sit above the F helix as viewed from the distal face (Fig. 5). The B–C loop includes three helical sections in P450 EpoK (labeled B'_1, B'_2, and B'_3 in Fig. 5). By sequence alignment, the last helical segment, B'_3, is best aligned with the canonical B′ helix in CYP101. Structurally, however, helix B'_2 appears to play the same structural role as B′ in CYP101. The double bond in the bound epothilone that is epoxidized is ~5 Å from the heme iron, a considerably longer distance than the 5-*exo* hydrogen that is abstracted from camphor in CYP101 (~3.5 Å). As with CYP107, it is likely that further rearrangement of the P450 EpoK structure is required to reach the catalytically competent conformation of the enzyme. However, examination of Figure 5 suggests that moving the B'_2 helix in towards the active site would force the F helix in the same direction and would uncross the F and G helices while moving the double bond to be epoxidized closer to the heme iron.

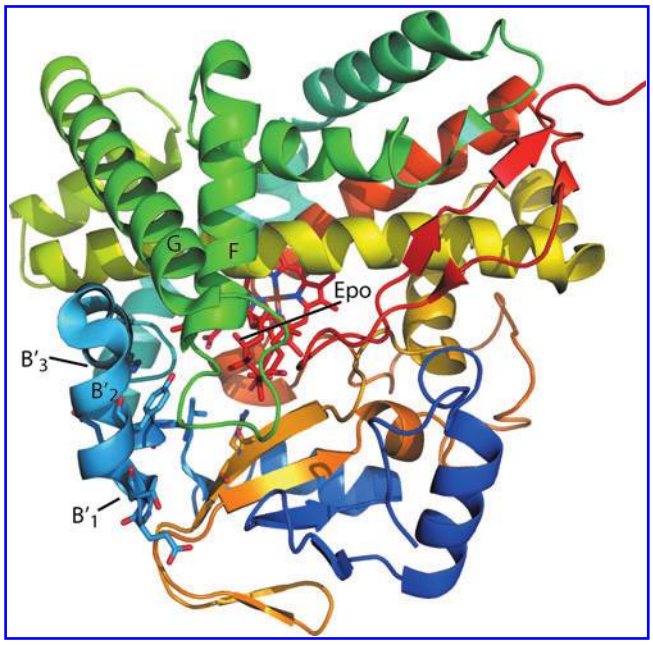

FIG. 5. Cytochrome P450 EpoK (PDB entry 1Q5D, (87)) viewed from distal face in the same orientation as CYP101 in Figure 1. Substrate (epothilone B, labeled Epo) (For interpretation of the references to color in this figure legend, the reader is referred to the web version of this article at www.liebertonline.com/ars).

D. Cytochrome $P450_{nor}$ (CYP55A1) and CYP105 (MoxA)

$P450_{nor}$ (for *n*itric *o*xide *r*eductase) is unusual among the P450s characterized to date in that it does not catalyze oxidative addition, but instead converts two NO molecules to N_2O using reducing equivalents from NADH. However, $P450_{nor}$ maintains the topology of the P450 superfamily and the structure is remarkably similar to that of bacterial P450s. The required NADH cofactor is bound with the adenine ring in a cleft between the B′, F, and G helices and the pyridoxal group located close to the heme iron, as determined from a structure with an NADH analog bound (91). CYP105 from the actinomycete *Nonomuraea recticatena* is structurally similar to CYP55A1, but unlike that enzyme, is a typical broad-spectrum P450, with roles in not only antibiotic biosynthesis but degradation of xenobiotics (165).

Recently, the engineering of another related enzyme, CYP105A1, was described. The wild-type enzyme from *S. griseolus* shows some ability to oxidize vitamin D_3 to the physiologically active form, 1α,25-dihydroxy-vitamin D_3. Hayashi *et al*. described a series of mutations in the B–C loop that generated forms of the enzyme that preferentially oxidized the position that was not oxidized (*i.e.*, 25-hydroxylation in the 1α-hydroxy product and 1α hydroxylation in the 25-hydroxylated) relative to the wild-type enzyme (38, 141). Interestingly, the crystal structure of the mutant enzyme with the dihydroxy vitamin D_3 bound (3CV9) shows the vitamin molecule aligned with the B′ helix, and well removed from the heme iron, with the 1α-carbon bound 11.9 Å and the C_{25} 13.5 Å from the heme iron.

E. Coupling reactions: CYP158, CYP121, and P450 OxyB

Given their ability to activate C-H and C-C bonds, it is not surprising that P450 enzymes play a role in mediating

oxidative coupling reactions. A series of structures by Waterman *et al.* illustrates an interesting case where two flaviolin molecules are bound in the CYP158A2 active site, where they are induced to undergo a coupling to generate a flavinoid (171). One flaviolin is in close proximity to the heme, while the other is stacked on top of the first, off-set and held in place by contacts with the B–C loop. In the CYP158A1 structure, two flaviolins are also bound, but instead of the close interaction observed in the CYP158A2 structure, one remains co-planar with the heme, while the other is ~9 Å away, bound between the B–C loop and the G helix (173). The two isoforms give rise to different ratios of bi- and tri-flaviolin products, and the authors discuss the roles of particular amino acid substitutions in determining the binding modes of the substrates.

CYP121 from *M. tuberculosis* was recently identified as catalyzing the oxidative coupling of tyrosine phenol rings in bis-tyrosyl diketopiperazine (7). This enzyme is of interest because it has been shown to be required for *M. tuberculosis* viability, but the role of the product of the reaction (C-C linkage between carbon atoms ortho to the phenol OH of the two tyrosine rings) is as yet unknown. In the structure determined with substrate bound (3G5H), the tyrosine rings that are coupled are quite remote from the heme iron (~6 Å from the carbon to be activated) as well as remote from each other (6.7 Å between the carbons to be coupled). The substrate interacts almost exclusively with the B′, F, and G helices, so these secondary structures must undergo considerable rearrangement in order to reach a catalytically competent form prior to reaction.

Perhaps the most atypical P450 structure determined to date is that of P450 OxyB (167). While the enzyme is expected to catalyze the tyrosine ring coupling involved in vancomycin synthesis, the reconstituted enzyme system does not give rise to product, suggesting that an additional co-factor or effector is required for activity *in vivo*. Unusually, the OxyB active site residues on the B–C loop and the β3 and β5 strands expected to contact substrate are prolines. In addition, nonrestrictive residues are present on the I helix. This suggests a fairly open but rigid active site involved in initial substrate binding (Fig. 6).

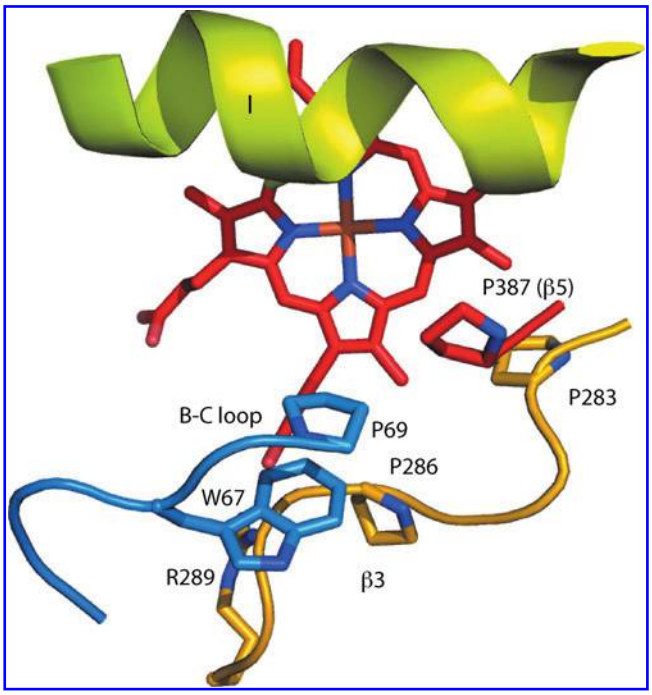

FIG. 6. Active site of P450 OxyB (PDB entry 1LFK, (167)) viewed from distal face in the same orientation as CYP101 in Figure 1. Unusually, most of the expected primary contacts for substrate vancomycin are prolines. (For interpretation of the references to color in this figure legend, the reader is referred to the web version of this article at www.liebertonline.com/ars).

III. Crystallographic Structures of Eukaryotic Cytochromes P450

A. Cytochromes P450 exported to the endoplasmic reticulum

This class of P450 enzymes, first identified in mammalian liver microsomal extracts, is of great interest in that they are responsible for oxidizing xenobiotics, including most compounds of pharmaceutical importance, to more soluble and excretable forms. They are for the most part reduced directly by NADPH-dependent flavoproteins, but it has been found that cytochrome b_5 acts as an effector for some P450s in this class, increasing the rate and efficiency of substrate oxidation (168).

These enzymes are typically membrane-bound, and as such have proven to be a challenge for structural biologists. In general, their structures have been determined using enzymes that have been modified to remove trans-membrane domains and (in a few cases) hydrophobic surface features that are likely involved in membrane association. The loss of N-terminal membrane binding domains will likely have little effect on the overall structures of these enzymes. However, many of these enzymes catalyze oxidations of compounds that probably enter the active site *via* the membrane with which the enzyme is associated. In such cases, the active site entrance is likely buried within the membrane, and the conformation of important structural features will be at least in part determined by interaction with the lipid environment. As will be seen, in the absence of a lipid bilayer, the conformations of the regions around the active sites of these enzymes show considerable variability depending on the presence/absence of substrate, substrate/inhibitor size, and other variables of the crystallization process.

The first enzyme in this class for which a crystal structure was solved was CYP2C5 (156). Although identified as a selective progesterone 21-hydroxylase, CYP2C5 was later found to oxidize a wide clientele of molecules (47). In order to obtain crystals, it was necessary to remove an N-terminal membrane anchor helix, as well as to make several mutations on the surface of the F helix and the F–G loop that reduce the tendency of the molecule to dimerize in solution. In the first structure (1DT6, Fig. 7), much of the F–G loop is disordered and no coordinates are reported for residues 212–222 in the F–G loop. Also, there is no regular secondary structure in the B–C loop, and the rigid turn-loop often found near the N-terminal end of the C helix is also absent. Along with four Gly residues in the B–C loop, this suggests that the B–C loop is considerably more flexible in this enzyme than in the prokaryotic enzymes for which structures had been determined to date. However, when complexed with dimethylsulfaphenazole (DMZ) (151), both loops become ordered: Two short

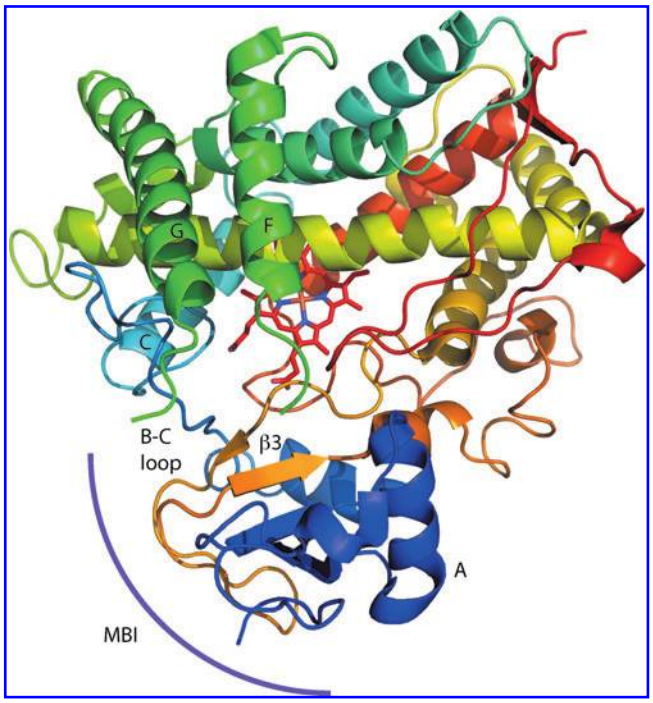

FIG. 7. Substrate-free CYP2C5 structure (1DT6 (47)) viewed from the distal face in the same orientation as CYP101 in Figure 1. Note that the F–G loop is disordered and there is no regular secondary structure in the B–C loop. The approximate location of the membrane binding interface including an N-terminal helix (not present) and portions of the F–G loop is marked as MBI. (For interpretation of the references to color in this figure legend, the reader is referred to the web version of this article at www.liebertonline.com/ars).

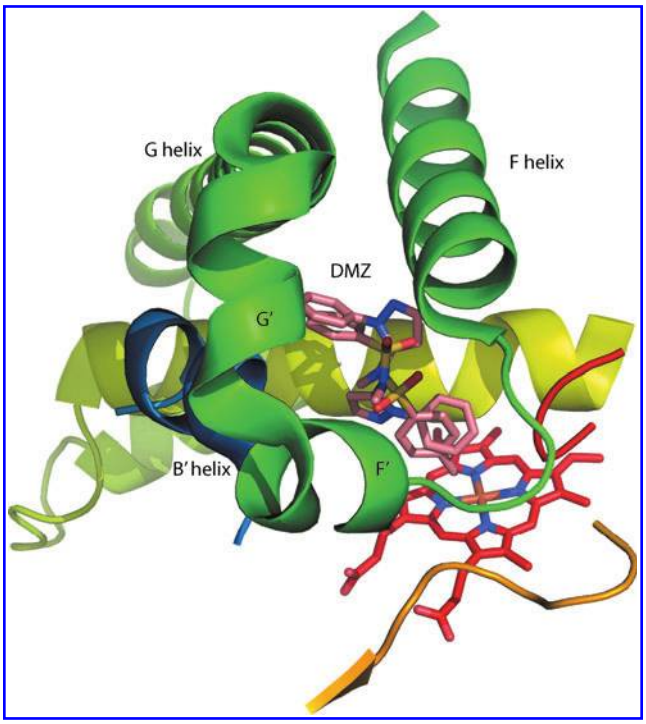

FIG. 8. CYP2C5 with substrate dimethylsulfathiazole (DMZ) bound in two orientations (1N6B (47)). The active site is viewed from the south edge. Note that the F–G loop is ordered and a short B′ helix is present, unlike the substrate-free form (Fig. 7). (For interpretation of the references to color in this figure legend, the reader is referred to the web version of this article at www.liebertonline.com/ars).

helices form immediately preceding the G helix, and a short B′ helix forms as well (Fig. 8). Interestingly, there is evidence for two DMZ binding modes in this structure, in which the substrate occupies the same volume, but is oriented in opposite directions. The pattern of hydroxylation observed for DMZ supports the two binding orientations (151). A third structure with a smaller substrate (diclofenac) present shows the same secondary structural features as the DMZ structure, but the B′, F, F′, and G′ helices are subtly rearranged to accommodate the small but more polar substrate molecule (152). Structures of the related CYP2C9 with anticoagulant *S*-warfarin bound show a similar arrangement of secondary structure in the F–G and B–C loops, but with a large vacancy in the active site directly above the heme iron in the site expected to be occupied by substrate. The authors have modeled in a second warfarin molecule, which fits readily into the vacancy, suggesting that further allosteric rearrangement or a second substrate binding event is required for the observed oxidations to take place (157).

Based on results from antigen peptide pattern recognition, it was proposed that the entrance to the active site of CYP2C5, as defined by the F–G loop, is embedded in the membrane *in vivo* (146). This would allow hydrophobic substrates to enter directly from the lipid bilayer rather than from the aqueous phase surrounding the membrane. Given that the F–G loop is disordered in the crystal of substrate-free CYP2C5, it is likely that the interaction between the lipid bilayer and residues that were mutated in order to permit crystals to be obtained is important in determining the overall shape and dynamics of the active site closure in CYP2C5 in the absence of substrate.

While the CYP2C5 and CYP2C9 structures show the basic topology of the P450 superfamily, a number of unusual features are observed. Neither CYP2C5 nor CYP2C9 have Arg residues in the usual position at one end of the β3 sheet in the south side of the active site (*vide infra*). In prokaryotic P450s for which structures have been determined, this Arg forms a salt bridge with a heme propionate, and anchors the β3 sheet in place at one end with respect to the heme and active site. Instead, in CYP2C5 an Arg residue from the β-meander region (Arg 430) forms a link between the two heme propionates, at least partially replacing the missing interaction. In CYP2C9, a similar role is played by an Arg residue from the B–C loop. In both CYP2C5 and CYP2C9, the β3 strand adjacent to the active site is very short, suggesting that the south wall of the active site has more freedom of movement relative to the heme than in enzymes in which the anchoring Arg residue is present.

B. CYP2B4

The rabbit liver microsomal enzyme CYP2B4 (originally P450 LM-2) was one of the earliest characterized mammalian cytochrome P450s, as its expression can be induced in rabbit liver by dosing with phenobarbital. The first published structure of CYP2B4 (131) showed an open active site, with the B′ helix removed from the active site (~22 Å from the

midpoint of the helix to the heme Fe) and a distorted helix (F′) serving as the F–G connector. The F′ helix is also remote from the heme iron, leaving a very large open active site partially occupied by water molecules. As with CYP2C5, the β3 strand is very short, and the Arg anchor is replaced by a histidine, suggesting that this interaction could be modulated by pH. A structure determined with 4-(4-chlorophenyl)imidazole bound shows a more compact active site, with residues from the B–C loop in contact with the bound substrate and the B′ helix close-packed (132). Recently, a structure with another inhibitor, 1-biphenyl-4-methyl-1H-imidazole, bound, resulted in an intimate dimer in which the F′ helices of each monomer occupies the active site of the dimer partner, interacting with the I helix of the partner, while a portion of the F–F′ loop forms a β-sheet with its counterpart in the other monomer (28). This indicates that structural features surrounding the active site of CYP2B4 are capable of very large displacements in response to environment.

C. Liver microsomal enzymes CYP3A4 and CYP1A2

The human liver microsomal enzyme CYP3A4 is of particular interest in that it is involved in the metabolism of many of the approved drugs currently marketed, and inhibition or unintentional overinduction (*e.g.*, by another drug or xenobiotic) can markedly affect the persistence, effectiveness, and toxicity of a particular drug (177). The client substrates of CYP3A4 vary significantly in size, and there is evidence for multiple substrates being bound simultaneously in the large active site (111). In one published structure (1TQN, (163)) without bound substrate in the active site, the B–C loop contains only a short distorted helical region, the F helix is considerably shorter than is typical, and the F-G loop contains two helical segments, the F′ and G′ helices (Fig. 9). Both of these helices expose hydrophobic residues expected to interact with the lipid bilayer of the membrane. The structure determined with erythromycin bound (2JOD, (25)) shows surprisingly little change in the overall structure of the active site: There is more disorder in the F–F′ region, but the same general arrangement of active site features are present. The erythromycin molecule binds slightly differently in the CYP3A4 active site than in P450 EpoK. The two sugar moieties of the substrate, instead of packing near the G helix and F–G loop as in EpoK, interact primarily with the F–F′ loop, the F′ helix, and portions of the A helix. The remainder of the substrate molecule interacts with the same structural features as seen with many other P450s, including the B–C loop, the I helix, and portions of the β3 and β5 sheets. With a smaller substrate (ketoconazole) bound so that the imidazole ring of ketoconazole provides an axial ligand to the heme iron, there is some ordering of the B–C loop where it interacts with substrate near the N-terminal end of the C helix (PDB entry 2V0M). However, despite the differences between erythromycin and ketoconazole structures, many of the same residues of CYP3A4 interact with both substrates, including the N-terminal end of the A helix.

The structure of another important drug-metabolizing P450, CYP1A2, has been determined with substrate naphthoflavone bound (2HI4, (126)). This enzyme, while broad spectrum, appears to target polycyclic substrates with significant planar groups (*vide infra*) (Fig. 10). As with CYP3A4, the F helix is short and somewhat irregular, while the F–G loop contains two short helical segments with exposed hydrophobic residues that likely interact with the membrane.

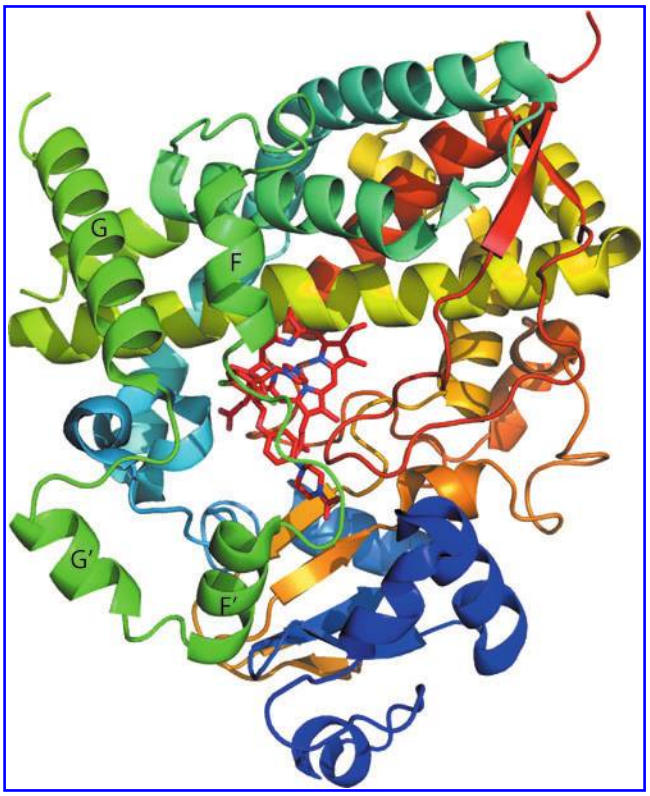

FIG. 9. Structure of CYP3A4 determined with inhibitor ketoconazole bound (2V0M (25)) viewed from the distal face in the same orientation as CYP101 in Figure 1. Note that the extended F–G loop with two helical regions F′ and G′. (For interpretation of the references to color in this figure legend, the reader is referred to the web version of this article at www.liebertonline.com/ars).

D. Prostaglandin biosynthesis: prostacyclin I2 synthase

The rearrangement of cyclic peroxide PGH2 to prostacyclin I2 is catalyzed by a P450 homologue, CYP8A1. While not a classical oxygen insertion, it seems likely that there is direct interaction between the peroxide oxygen and the heme, as one structure with a substrate analog bound has one nitrogen of the imide analog of the peroxy oxygen bound to the heme iron (3B99, (68)). There are three published structures of CYP8A1 from zebrafish and human. All three structures, including that without substrate analog or inhibitor bound, show a well-defined B′ helix, as well as a short F′ helix connecting the F and G helices. The β5 sheet is poorly defined near the active site, and one β5 strand is interrupted by a short helix. The substrate analog in 3B99 is contacted by strongly constraining residues (Trp 272 and Val 273 on the I helix, Phe 465 from the β5 loop, and Tyr 97 from the B′ helix). As might be expected, there is some resemblance of the arrangement of structures near the active site to the structure of CYP102, which also binds fatty acid derivatives; however, this may be coincidental.

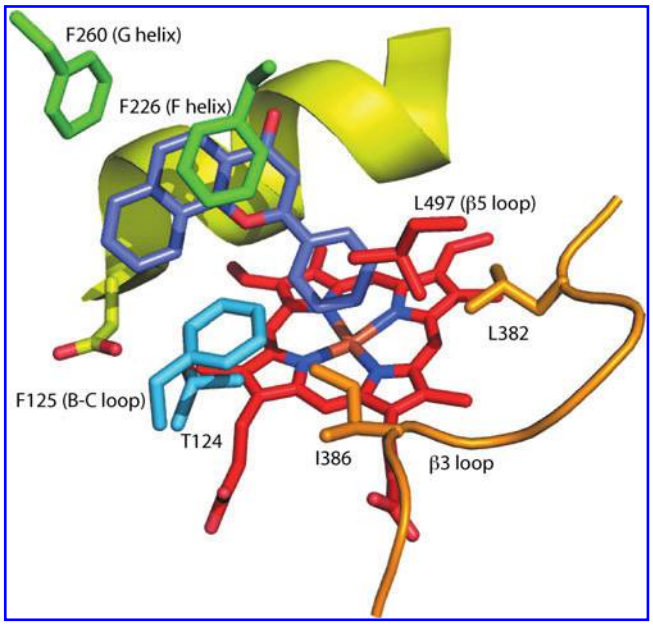

FIG. 10. Active site of CYP1A2 with substrate naphthoflavone bound (2HI4, (126)). Naphthoflavone carbon atoms are shown in *purple*. (For interpretation of the references to color in this figure legend, the reader is referred to the web version of this article at www.liebertonline.com/ars).

E. Steroid biosynthetic and catabolic enzymes

Until recently, there were no structures determined for P450s involved in steroid biosynthesis, even though members of this class were among the earliest identified and characterized in humans. This has changed with the publication of structures for CYP46A1 (cholesterol 24-hydroxylase) (79) and human aromatase (CYP19A1) (29). CYP46A1 was characterized both with and without substrate (cholesterol sulfate) bound, and shows increased order in the F–G loop and inward movement of the B′ helix in the substrate-bound form. Aromatase catalyzes the oxidative C-19 demethylation and aromatization of the steroid A ring, converting androstene dione to estrone, testosterone to estradiol, and hydroxytestosterone to estratriol. Aromatase inhibitors are primary therapies for estrogen-dependent breast cancers, making this structure of particular interest for rational drug design. The aromatase structure was the first to be determined using protein derived from mammalian tissue, as opposed to heterologously expressed enzyme. The enzyme was purified from human placenta *via* immunoaffinity chromatography, and presumably contains the intact membrane-binding N-terminal residues, although diffraction was not observed for the first 45 residues in the enzyme. There is evidence that CYP19A1 is glycosylated near the N-terminus *in vivo*, and the glycosylation may act as an anchor on the opposite (lumen) side of the membrane from the protein (29). Three distinct reactions are catalyzed by aromatase, two of which (the oxidation of C-19 methyl to primary alcohol to aldehyde) can be rationalized by a standard P450 mechanism involving a high-valent Fe-oxo species. To rationalize the final step in the reaction, the authors invoke proton abstraction from the A ring by a Fe^{+3}-bound peroxide intermediate that facilitates loss of the 19-C aldehyde *via* deformylation.

Another enzyme involved in steroid metabolism is CYP125 from *M. tuberculosis* (82). The active site of the enzyme would be expected to pack a cholesterol molecule close to the I helix, as Phe residues from the β3 and β5 strands provide considerable steric restraints deeper within the active site. However, a molecule of andostenedione in structure 3IW1 is bound remote from the heme between the B′ and G helices, so considerable reorganization of the complex must occur prior to catalysis.

F. Computational modeling of P450 structures

Given the advances that have been made in recent years in homology modeling of protein structures, combined with the historical paucity of determined P450 structures, it is inevitable that a good deal of effort has gone into predicting tertiary structure of new P450 sequences from existing structures. On one hand, this makes sense: The highly conserved (and yet apparently unique) P450 core folding topology makes modeling an unknown structure straightforward and the resulting model probably accurate, at least to the level of folding topology. On the other hand, given the plasticity and variation of active sites seen even among different structures of a single isozyme (28, 131, 132, 175, 176), assessing the accuracy and utility of active site structures obtained by modeling is difficult, and using sequence alignments to predict such structural variables as helix and loop orientations, particularly in the B–C and F–G loop regions, somewhat risky (58). This area has been reviewed thoroughly, particularly from the point of view of modeling substrates and inhibitors into target P450 structures, with an eye towards establishing quantitative structure–activity relationships and identifying critical residues for mutation studies (4, 19, 40, 45, 59–61, 147, 178).

IV. Nuclear Magnetic Resonance as a Probe of Cytochrome P450 Structure and Dynamics

Nuclear magnetic resonance (NMR) provides a useful complement to crystallographic methods for characterizing the structure of biological macromolecules. While the *de novo* determination of a cytochrome P450 structure by NMR methods has not been reported, it has been shown that extensive sequential resonance assignments (a prerequisite for structure determination) can be made for soluble P450s (5), and high-quality solid state NMR spectra have been demonstrated for membrane-associated mammalian P450s as well (51). NMR methods often require a significant investment of time and resources to reach the point at which interpretable atomic resolution information concerning structure and dynamics of P450 can be obtained: Isotopically labeled samples must be prepared of sufficient concentration and purity for spectroscopy, a variety of multidimensional NMR experiments performed, and then sequential assignments must be made. P450 enzymes are sufficiently large that the automated assignment methodologies employed for smaller proteins are not particularly useful, and much of the assignment work must be done by hand. However, the repayment for the investment is handsome: With sequential assignments in hand, it is possible to identify discrete conformational changes that are associated with enzyme function, and to localize structural perturbations resulting from substrate and effector

binding and changes in oxidation state (95). Equally important, protein dynamics on a wide range of time scales becomes accessible via NMR methods (98).

One of the earliest NMR studies to relate structure and function in cytochromes P450 was published by the Roberts group (84). Based on the paramagnetically-induced spin relaxation of water and substrate (lauric acid) in the CYP102 active site, this group was able to identify a 6 Å relocation of the substrate upon reduction of the enzyme, and used this information combined with the published crystallographic structure of CYP102 to generate models for the binding of lauric acid in oxidized and reduced CYP102. The same group has applied this methodology successfully to other P450-substrate complexes as well (83, 120–122). Note that this work did not require sequential assignments of the protein resonances; only the substrate ^{1}H resonances were assigned, and paramagnetic relaxation of specific resonances in substrate were sufficient (in combination with the crystal structure of CYP102) to model the active site structure. Similar efforts have used relaxation to examine substrate and ligand-heme interactions with other P450s, including CYP1A1, CYP2B1, (85) CYP3A4 (10), CYP2C9 (44), and CYP2B4 (80).

Our group has used NMR to investigate the solution conformation of the camphor monooxygenase CYP101 as a function of oxidation state, effector binding, and substrate. It has long been known that the $Cys_4Fe_2S_2$ ferredoxin putidaredoxin (Pdx) is a required component of the reconstituted camphor hydroxylase enzyme system: In the presence of Pdx, reduced O_2- and camphor-bound CYP101 rapidly turns over to yield 5-*exo*-hydroxycamphor (70). In the absence of Pdx, the same complex slowly decomposes to yield superoxide anion and resting state enzyme. In light of this, the published structures of camphor-bound CYP101 presented an interesting puzzle. These structures give an obvious rationale for the observed regio- and stereochemistry of camphor hydroxylation by CYP101. C5 of camphor, where the hydroxylation occurs, is the closest substrate carbon to the heme iron, and so also to the presumed reactive intermediate, the high-valent iron-oxo species Fe(IV) = O. A time-resolved series of structures in which the hydroxylation reaction was photochemically induced clearly demonstrated the position of the substrate with respect to the metal center during the reaction sequence (128). Based on these structures, the lack of turnover in the absence of Pdx was puzzling. Furthermore, the question of how the substrate gets into the active site and how product is expelled presented difficulties. The B′ helix and F–G loop provide effective closure to the CYP101 active site in all CYP101 structures. A series of dynamic simulations of substrate expulsion suggested a number of possible paths for active site ingress/egress, but all of them clearly require significant displacements of distal structural features in order to permit access to the active site from solvent (71, 72). Now, many of these issues can be resolved by the results from multidimensional solution NMR experiments. Preliminary titrations of camphor bound CYP101 with Pdx showed that, despite the proposed Pdx binding site being on the proximal face of the molecule (100), many distal features, including the B′, F, G, and I helices are perturbed upon Pdx addition (99). We proposed these observations to be the result of a Pdx-enforced selection of a closed conformation of the enzyme that prevents substrate/intermediate loss during the final steps of oxygen activation and hydrogen abstraction from substrate. Repeating the titration with perdeuterated CYP101 and Pdx (which renders both proteins invisible to ^{1}H NMR) allowed a detailed characterization of substrate orientation in the active site, and demonstrated that the orientation of camphor substrate in the CYP101 active site differs between solution and the orientation observed in crystal structures (149). Furthermore, a slow conformational change driven by Pdx binding ($\sim 180\,s^{-1}$ at half-saturation) was detected that coincided with substrate reorientation, suggesting that a coordinated conformational switch occurs upon Pdx binding. Spectroscopic and mutagenic evidence identified the hinge of the conformational change as a *trans-cis* isomerization of the peptide bond between Ile 88 and Pro 89, at the N-terminus of the B′ helix (95). This bond is in the *cis* conformation in all CYP101 crystal structures, but adopts a *trans* or distorted *trans* conformation in solution. Dynamic simulations show a wider gap between Phe 87 and Pro 89 on the B–C loop, Thr 185 on the F–G loop, Phe 193 on the G helix, and Ile 395 on the β5 strand at the entrance to the active site. The *trans* structure shows greater solvent exposure of substrate, as well as reorientation of substrate relative to the crystal structure, in agreement with earlier NMR results (5) (Fig. 11). Taken together, these results suggest that upon crystallization, CYP101 packs most efficiently in a compact, closed (*cis*) conformation, but in solution adopts a more open set of *trans* conformers that permit relatively easy substrate access and product egress from the active site. Upon effector binding, the *cis* conformer predominates, yielding the closed, catalytically competent form of the enzyme.

Other publications describing the use of solution state NMR methods to characterize P450 enzymes have also appeared. Yao *et al.* have proposed a second camphor binding site on CYP101 based on ^{1}H NMR relaxation evidence (164). Jain and co-workers have proposed a model for Pdx-CYP101 interactions based on spin label-induced relaxation and residual dipolar couplings (170). Roberts and co-workers used selective ^{15}N labeling of phenylalanine residues to examine substrate binding modes in P450 EryF (120), and Morishima *et al*. have conducted extensive combined NMR and mutagenesis experiments to understand the role of Pdx binding in driving conformational changes in CYP101 (89, 142, 143).

As most eukaryotic P450 enzymes are membrane-bound, solution state NMR methods are at present limited in applicability to this large and interesting class of targets. However, combined with selective and uniform isotopic labeling, recent developments in solid-state NMR methods promise to make eukaryotic P450s more accessible (51, 124). Using solid state NMR, the McDermott group has shown that substrate binding and spin state in CYP102 is temperature dependent, suggesting substrate reorientation as a function of temperature in that enzyme (48, 49). Rienstra and co-workers have demonstrated that good quality solid-state ^{13}C correlation spectra can be obtained for native CYP3A4 bound to size-constrained phospholipid bilayer structures known as "nanodiscs" (51).

V. Structural and Dynamic Insights from Mass Spectrometry

Although not precisely a structural tool, mass spectrometry (MS) offers another alternative for examining structural and dynamic relationships in cytochromes P450 that shows considerable promise. Recent developments in desorption and

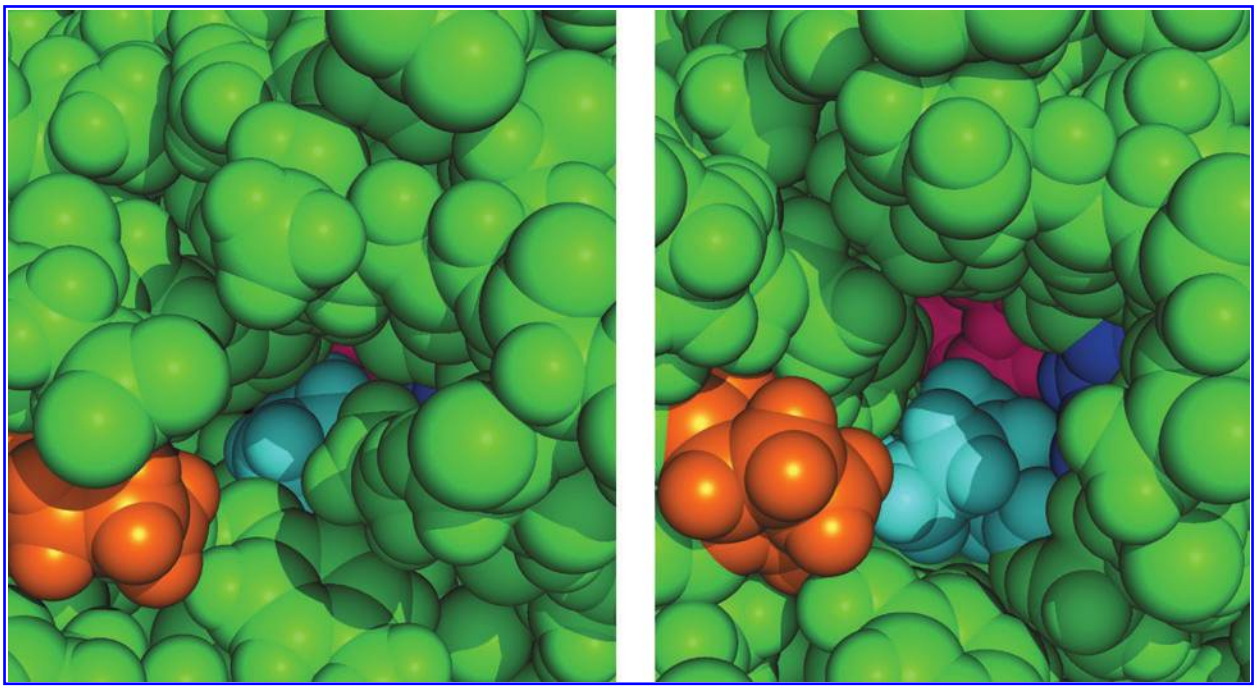

FIG. 11. Comparison of the *cis* (*left*) and *trans* (*right*) conformations of the Ile 88-Pro 89 amide bond initiating the B′ helix in CYP101. Structures shown are based on molecular dynamics simulations supported by NMR experiments (5). Pro 89 is shown in *orange*, Ile 395 in *light blue*, Thr 185 in *dark blue*, and camphor (substrate) is in *magenta*. Note the greater solvent exposure of camphor in the *trans* conformation, indicating a more accessible active site. (For interpretation of the references to color in this figure legend, the reader is referred to the web version of this article at www.liebertonline.com/ars).

ionization of intact proteins, as well as proteomic analysis using fragmentation and MS/MS techniques, have rendered the P450 superfamily amenable to sequence-activity analysis. While small-molecule mass spectrometry has long been used as a tool for characterizing products of P450-mediated oxidations, the ability to rapidly pre-digest intact proteins prior to introduction to the mass spectrometer has allowed mass spectrometry to be used to identify sites of covalent modification associated with suicide substrates, as well as examine local protein dynamics as a function of such parameters as oxidation state and substrate binding.

A number of published examples illustrate the potential of the methodology. Sites of photoaffinity label attachment in CYP3A4 have been determined by mass spectrometry, helping to clarify active site accessibility (150). We have used hydrogen–deuterium (H/D) exchange methods coupled with MS/MS to examine the dependence of local protein dynamics on the oxidation and ligation state of the heme in CYP101. We found that portions of the β3 and β5 sheets, the B′ and I helices (that is, most of the secondary structures surrounding the active site) all show differential H/D exchange in response to changes in the heme oxidation/ligation state (35, 98). Other recent publications deal with the effect of substrate and effector binding to CYP46A1 using H/D exchange (69) and identification of membrane binding domains (78).

VI. Can We Identify Structural Motifs in P450 Structures That Correlate with Activity?

Given the number of nonredundant P450 primary sequences that have been described and deposited in such databases as GenBank and SwissProt, it is difficult to imagine solving structures for more than a tiny fraction of these enzymes. We are then left with an important question: Can we find common threads whereby we can correlate sequence in the structurally variable regions of P450 enzymes, if not with a particular substrate, then with a particular kind of activity? We have previously suggested a simple example of this type of correlation with our identification of a *trans-cis* isomerization of an Ile-Pro bond preceding the B′ helix in CYP101. The isomerization is driven by binding of an effector, Pdx (*vide supra*), and results in apparent closure of the active site access channel and repositioning of substrate into the correct orientation for the observed chemistry (5, 95) (see Fig. 11). P450 structures determined to date in which a hydrophobic residue (hϕ = Phe, Ile, Val, Leu) precedes a proline at the beginning of the B′ helix include CYP101, CYP119, CYP107 (EryF), and CYP121 that catalyzes tyrosyl diketopiperazine coupling in *M. tuberculosis*. In this enzyme, the substrate, which interacts strongly with the B′ helix in the crystal structure, is quite remote from the heme iron, and isomerization of the Val-Pro bond offers a mechanism for bringing substrate close to the heme iron. This motif is also found in the B–C loop of CYP2C5 and CYP2C9, and initiates the B′ helix in the substrate-bound forms (151, 152, 157). In P450 EpoK, the hϕ-Pro motif is found at the beginning of the B'_3 helix. All of these enzymes either target specific substrates and/or are regio- and stereospecific in the oxidations that they catalyze. This suggests that effector-driven isomerization of this bond, along with the corresponding translocation of the B′ helix, is the final step in locking the substrate in the correct orientation for the observed regio- and stereochemistry. This isomerization also prevents loss of substrates and intermediates during the catalytic process. In

turn, this simple structural motif may provide a marker for identifying P450 enzymes that are specific for particular substrate/product combinations. Other enzymes, while lacking this motif in the B–C loop, have Ile-Pro initiating the F′ helix in the F–G loop. In the structure of lanosterol 14-α demethylase CYP51 (PDB entry 3GW9) from *T. brucei*, in which an inhibitor is bound to the heme iron, the active site is quite exposed to solvent. However, modeling suggests that isomerization of the Ile 209-Pro 210 amide bond at the N-terminal of the F′ helix from *trans* to *cis* would close the active site in a manner similar to the CYP101 case. A similar arrangement of Leu-Pro is seen initiating the F′ helix in allene oxide synthase from *A. thaliana* (55, 65), and Phe-Pro is present in the F–G loop of PikC (67). There are, however, enzymes that do not have an hϕ-Pro motif but still target specific substrates: CYP108, that oxidizes α-terpineol, is one example, so clearly this is not the only means by which stereo- and regiospecificity can be enforced.

Regardless of the precise mechanism, it is reasonable to assume, based on comparisons of multiple P450 structures, that the B–C loop, the F and G helices, and F–G loop must rearrange in order to generate a closed conformation once substrate is bound. This implies that substrate contacts from these secondary structural features are less important for initial substrate recognition than for determining the final "correct" orientation of the substrate in the competent enzyme complex. A similar conclusion was reached by Lepesheva *et al.* based on a series of mutations made in the B–C and F–G regions of CYP51, a sterol demethylase found in a wide range of organisms (58).

In CYP101, residues Phe 87, Tyr 96, and Phe 98, which contact substrate in the closed conformation from the B–C loop and B′ helix, would interact with substrate after binding, while substrate contacts from the I helix (Leu 244 and Val 247) and the β3 and β5 sheets (Val 295, Ile 395, and Val 396) are more likely involved in initial substrate binding and recognition. In light of this, it is worth considering how the arrangement of residues in these features might control initial substrate recognition. In the promiscuous CYP3A4, residues protruding into the active site are not bulky or constraining: Close contacts (within 5 Å) of ketoconazole in the CYP3A4 active site are alanines on the I helix and at the N-terminal of the β3 sheet that borders the active site to the south, as viewed in Figures 1 and 9. The same two I helix residues are also alanines in the EpoK structure (Ala 250 and Ala 254), allowing the bulky macrolide substrate to pack close to the I helix. However, the side chains projecting from the β3 and β5 strands in EpoK are bulky and

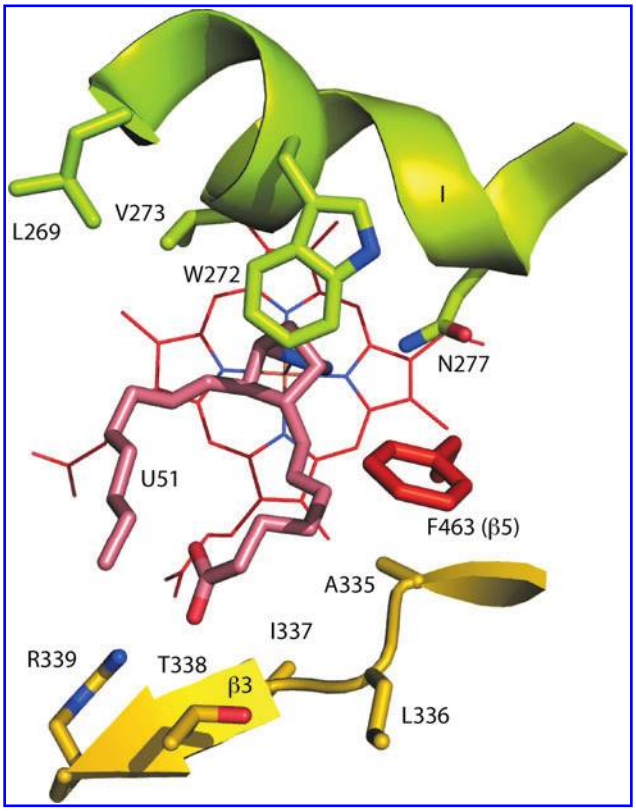

FIG. 12. Active site structure of prostacyclin synthase, CYP8A1 (PDB ID 3B99, (68)) with substrate analog 9,11-azoprosta-5(*Z*),13(*E*)-dien-1-oic acid bound (labeled U51 in figure). (For interpretation of the references to color in this figure legend, the reader is referred to the web version of this article at www.liebertonline.com/ars).

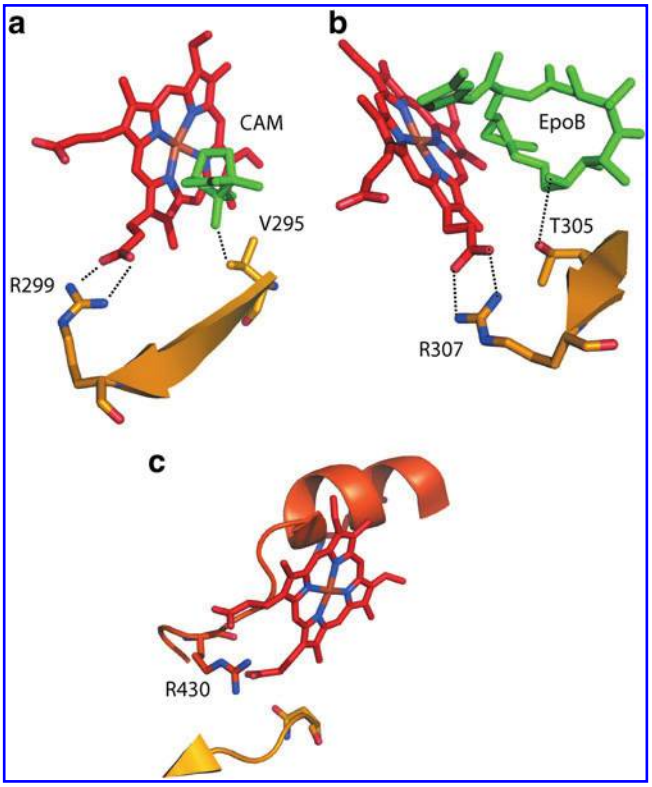

FIG. 13. Anchoring of β3 strand at the south edge of the active site by a salt bridge between the heme propionate and conserved Arg residues in (a) CYP101 (2CPP, (109)), and (b) P450 epoK (1Q5D, (87)). Substrate contact residues in register with the conserved Arg are Val 295 in CYP101 and Thr 305 in P450 EpoK. Substrates are camphor in CYP101 and epothilone B (epoB) in EpoK. See text for complete discussion. In (c) CYP2C5 (1NR6, (156)), the Arg is not present in the β3 strand, but the salt bridge is conserved via Arg 430 from the proximal side of the enzyme. (For interpretation of the references to color in this figure legend, the reader is referred to the web version of this article at www.liebertonline.com/ars).

restrictive, unlike CYP3A4, reducing the size of the active site cavity and the freedom of movement of substrate. In CYP1A2, another broad-spectrum xenobiotic metabolizing enzyme, the I helix residues are still nonrestrictive (Gly and Asp), but bulkier side chains project from the β3 and β5 strands to contact the substrate (α-naphthoflavone) and hold the polycyclic planar substrate perpendicular to the heme and parallel to the I helix (Fig. 10). Aromatic residues on the B′, F, and G helices also interact with the substrate, and fix its orientation quite precisely (126). A similar arrangement of interactions involving substrate, the I helix and the β3 and β5 strands is found in CYP2A6 (161). CYP108, which selectively oxidizes α-terpineol, also has a nonrestrictive alanine on the I helix that likely contacts substrate, while likely primary contacts on the β3 and N-terminal extension include phenylalanine and valine, and a phenylalanine on the β5 strand (37). In CYP8A1, which catalyzes the rearrangement of the cyclic peroxide PGH2 to prostacyclin PGI1, close contacts with substrate analog are provided by Trp 272 and Val 273 on the the I helix and Phe 463 on the β5 strand (68) (Fig. 12).Again, sterically restrictive β-branched and aromatic residues provide the initial contacts for substrate.

If contacts from the β3 sheet are important in the initial binding and recognition of substrate, this provides another potential correlation between active site structure and function in P450s. In most prokaryotic and many eukaryotic P450s, the β3 strand that borders the active site ends with an Arg residue that provides a salt bridge to one heme propionate group. In CYP101, this is Arg 299. This salt bridge essentially fixes one end of the β3 sheet with respect to the heme and active site via a flexible hinge. Interestingly, if this Arg residue is present, the other end of the β3 strand often has a residue in register with the Arg side chain that makes contact with substrate. In CYP101, this is Val 295, the side chain of which makes direct contact with the camphor geminal methyl groups (Fig. 13a). In P450 EpoK, a threonine (Thr 305) fills this role, with Arg 307 providing the anchor (Fig. 13b). In the recently published aromatase structure with bound androstenedione, Arg 375 and Val 373 are seen at homologous positions (29). For enzymes with larger substrates, the Arg anchor and contact residues from the β3 strand are often two residues apart, while in CYP101, with a small substrate, they are four residues apart. This suggests that the larger spacing between the Arg and contact residue moves the substrate deeper into the active site; that is, the length of the strand depends upon the size of the substrate, and that this contact is important for determining where the substrate sits in the active site relative to activated Fe=O species. In cases where the spacing is short, (two residues instead of four), the N-terminal continuation of the polypeptide that creates the edge of the β3 sheet often provides a portion of the east wall of the active site. The inward facing residue of this loop then becomes a key contact for substrate as well.

If very large or extended substrates are bound, the residue immediately adjacent to the conserved Arg is often involved. In CYP46A1, cholesterol 24-hydroxylase, the primary substrate contact residue, Phe 371, is immediately adjacent to the hinge Arg 372, but interacts with the substrate (cholesterol sulfate) on the A ring far from the site of hydroxylation. The N-terminal continuation on the east wall of the active site provides a bulky tryptophan side chain (Trp 368) that provides significant restriction on motion of the substrate in the active site (79). Interestingly, a similar situation is seen in aromatase: in this case, the residue adjacent to Arg in the β3 strand is methionine, which contacts the androgen D ring,

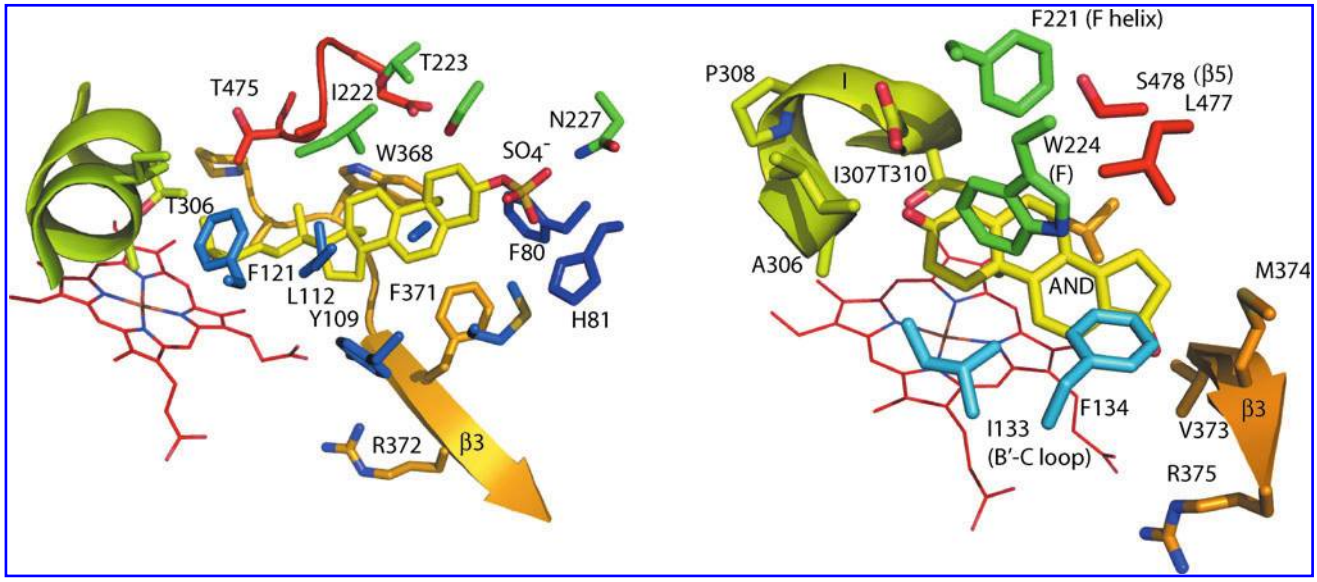

FIG. 14. Active sites of two P450 enzymes that bind cholesterol-derived substrates in opposite orientations. (*Left*) Active site of CYP46A1 with cholesterol sulfate bound (2Q9F, (79)). Side chains in *dark blue* are from the A helix, *light blue* from the B–C loop, *green* from the F helix and F–G loop, *orange* from the β3 strand and loop, and *red* from the β5 loop. (*Right*) Active site of aromatase with substrate androstenedione bound (CYP19A1, PDB ID 3EQM, (29)). Side chains in *light blue* from the B–C loop, *green* from the F helix, *orange* from the β3 strand and loop, and *red* from the β5 loop. Note the unusual Pro in the I helix, P308, which appears to make the "kink" often found in the I helix providing a binding site for bound O_2. (For interpretation of the references to color in this figure legend, the reader is referred to the web version of this article at www.liebertonline.com/ars).

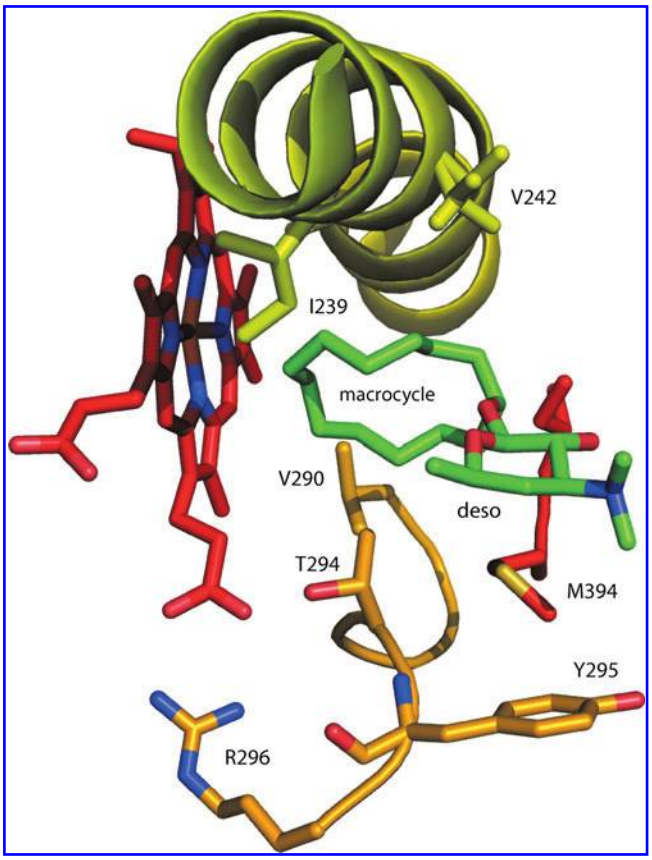

FIG. 15. View from west side of the active site of CYP107L1 (PikC) from structure 2WHW (67) showing side chains from the I helix, β3 and β5 loops involved in binding a substrate modified with a desaminoglucoside (deso) to convert a C_{13} macrocycle into a substrate for oxidation by this enzyme. The desaminoglucoside binding site is defined by Tyr 295 and Thr 294 on the β3 loop and Met 394 on the β5 loop. The desaminoglucoside is also contacted by Glu 94 on the B–C loop and Phe 178 on the F helix (not shown). Other marked residues (Ile 239 and Val 242 on the I helix, and Val 290 on the east wall of the active site) contact the macrocycle. (For interpretation of the references to color in this figure legend, the reader is referred to the web version of this article at www.liebertonline.com/ars).

CYP101		V	A	A	G	R	299
EpoK		I	G	T	V	R	307
aromatase		D	L	V	M	R	375
CYP46A1		W	G	T	F	R	372
PikC		S	A	T	Y	R	296
CYP120A1		G	G	G	F	R	323
CYP3A4	A	M	R	L	E	R	375
CYP2C5	P	T	N	L	P	H	365
CYP2C8	P	T	G	V	P	H	368
CYP2B4	P	F	G	V	P	H	369
CYP1A2	P	F	T	I	P	H	388
CYP2E1	P	S	N	L	P	H	370

FIG. 16. Alignment of β3 regions lining the active sites of P450 enzymes discussed in the text. Numbers to the right of the aligned sequences are sequence number of the aligned Arg/His residues from each sequence.

while the N-terminal continuation contact is a valine (Fig. 14) (29). Note that the steroid molecules bind to the two enzymes in opposite orientations; the increased steric bulk of the phenylalanine and tryptophan in CYP46A1 relative to the methionine and valine in aromatase appears to be important for this discrimination. In CYP107L1 (PikC), the desosamine binding site is formed by contacts from Thr 294 and Tyr 295 adjacent to the conserved Arg 296, as well as Met 394 in the β5 loop (Fig. 15).A phenylalanine adjacent to the conserved Arg contacts the bound retinoic acid in CYP120A1, as does a valine with epothilione B in CYP EpoK, providing stabilization of large substrates remote from the heme pocket.

On the other hand, in promiscuous enzymes that bind multiple substrates, the β3 strand is often very short, and the Arg at the C-terminal end of the strand often replaced by a His residue (*vide supra*) as in CYP2C5 (Fig. 13c), CYP2C8, CYP2B4, CYP1A2, and CYP2D6. This motif also includes two conserved prolines, one immediately preceding the His by five residues, and the second immediately preceding the conserved His (Fig. 16).The Arg is present in CYP3A4 (Arg 375), and there is a leucine in register (Leu 373). However, the side chain of Leu 373 does not extend into the active site, but rather projects past the heme plane to the proximal side of the enzyme. In CYP2E1, which targets primarily smaller substrates, the Arg is again replaced by His (His 370), with Leu 368 in register and Val 364 in the east wall, with Phe 298 from the I helix and Phe 478 from the 5 loop both protruding into the active site, restricting considerably the size of potential substrates.

Consider the case of CYP119, a thermostable P450 for which the natural substrate is unknown, but which has the

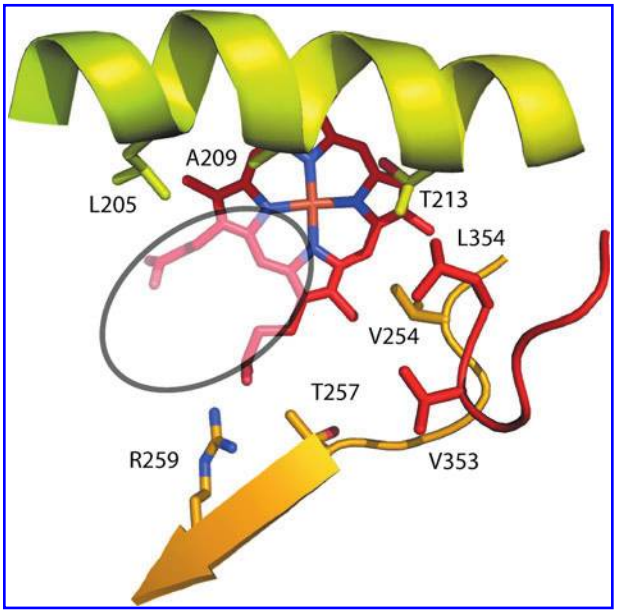

FIG. 17. Active site of CYP119, from *S. solfataricus* (PDB ID I1O8, (97)), showing positions of active site residues proposed to be important for substrate recognition and binding. *Translucent oval* shows approximate position proposed for bound substrate. (For interpretation of the references to color in this figure legend, the reader is referred to the web version of this article at www.liebertonline.com/ars).

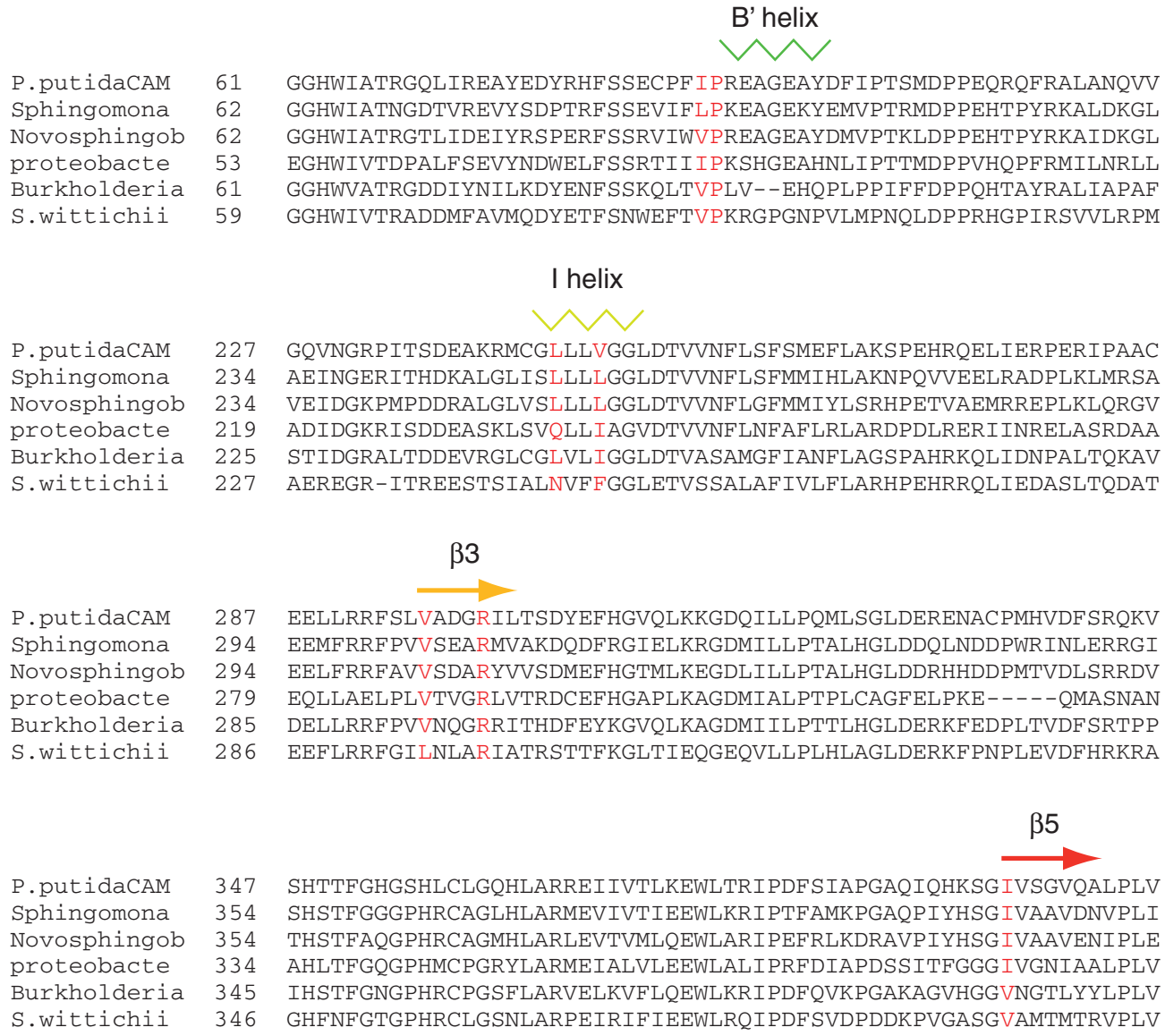

FIG. 18. Partial sequence alignments of selected putative P450 sequences with cytochrome P450cam (CYP101) from *P. putida* showing correlations discussed in text. Secondary structural features are noted above the CAM sequence. GenBank accession numbers are as follows: ZP_01304513.1 *Sphingomonas* sp. SKA58, YP_495795.1 *Novosphingobium aromaticivorans*, ZP_04956740.1 gamma proteobacterium, YP_001774457.1 *Burkholderia cenocepacia*, YP_001262244.1 *Sphingomonas wittichii*. Alignments were made using the BLAST alignment tool (blast.ncbi.nlm.nih.gov) (2). (For interpretation of the references to color in this figure legend, the reader is referred to the web version of this article at www.liebertonline.com/ars).

ability to catalyze the ω-1, −2 and −3 hydroxylation of lauric acid (52) and the peroxide-supported oxidation of styrene, phenanthrene, and biphenylene (52). The B′ helix in CYP119 is initiated by an Ile-Pro motif, suggesting that the enzyme catalyzes a regio- and/or stereoselective oxidation *in vivo*. The β3 strand is shorter than in CYP101, with a spacing of two residues between the Arg anchor (Arg 259) and Thr 257, the putative substrate contact. This suggests that the substrate is not bound deeply in the active site, so that oxidation occurs at either one end of the molecule or at a bend or oblate edge (Fig. 17). The absence of a hydrophobic residue immediately adjacent to the conserved Arg indicates that the natural substrate is not steroidal nor does it have bulky pendant groups remote from the site of oxidation. Bulky groups (Leu 205 and Leu 206) on the I helix as well as valines on the N-terminal loop of the β3 strand and the β5 bend suggest a relatively narrow binding site, one that might accommodate an aromatic ring or bent hydrocarbon chain. A phenylalanine from the F helix (Phe 153) and Leu 69 from the B′ helix would be expected to contact substrate after active site closure, further restricting the size of the molecule to be bound. All of these observations are consistent with the observed substrate selectivity of CYP119. Unfortunately, the context of CYP119 in the *Sulfolobus* genome is relatively uninformative concerning the natural substrate, as most of the neighboring open reading frames are not yet annotated (12).

An arrangement of active site residues similar to those in CYP119 is also found in CYPBioI, which oxidizes fatty acids at

Table 1. Cytochrome P450 Structures Accessible in the RCSB PDB Database

Enzyme	*Protein Data Base Entries*	*Organism*	*Substrate/Product (if known)*	*References*
CYP101 (cam)	(2-8)CPP, 3FWF-J, 2QBL-O, 2GQX, 2GR6, 2FRZ, 2H7Q-S, 2FE6, 2FER, 2FEU, 2A1M-O, 1UYU, 1T85-8, 1O76, 1LWL, 1K2O, 1GJM, 1DZ4, 1DZ8-9, 1DZ6, 5CP4, 6CP4, 1AKD, 1FAG-H, 1OXA, 1PHA-G, (1-4)CP4	*P. putida*	Camphor/5-exo-hydroxycamphor	1, 22, 23, 26, 75, 76, 88, 108-110, 113-118, 128, 129, 144, 145
CYP102 (BM3)	3HF2, 3DGI, 3EKB, 3EKD, 3EKF, 3BEN, 3CBD, 2UWH, 2J1M, 2J4S, 2IJ2-5, 2IJ7, 1Z04, 1Z09,1Z0A, 1YQO-P, 1SMI-J, 1P0V-X, 1JME, 1JPZ, 2BMH, 2HPD	*B. megaterium*	Fatty acid ω-2-hydroxylase	14, 30, 31, 33, 34, 39, 43, 63, 64, 92, 93, 119, 154, 166
CYP105 (MoxA)	2Z36	*Actinomycetes*	Broad specificity	165
CYP105A1	3CV8, 3CV9, 2ZBX-Z	*S. griseolus*	Vitamin D	38, 141
CYP105P1	3E5J-L	*S. avermitilis*	Filipin	158
CYP107 (EryF)	1Z8O-Q,1JIN-P, 1EUP	*S. erythreae*	6-Deoxyerythronolide B hydroxylase/ Erythromycin D	16–18, 86
CYP107L1 (PikC)	2VZ7, 2VZM, 2CD8, 2CA0, 2BVJ, 2C6H, 2C7X, 2WHW, 2WI9	*S. venezuelae*	Pikromycin, narbomycin	67, 135
CYP108 (terp)	1CPT	*P. putida*	α-Terpineol	37
CYP113A1 (EryK)	2WIO, 2JJN-P, 2VRV, 1EGY	*S. erythreae*	Erythromycin D	127
CYP119	1IO7-9, 1F4T-U	*S. solfataricus*	Unknown	97, 162
CYP120A1	2VE3-4	*Synechosystis*	Retinoic acid	54
CYP121	3G5F, 3G5H, 3CXV-Z, 3CY0,3CY1, 1N40, 1N4G	*M. tuberculosis*	Tyrosine diketopiperazine coupling	7, 62, 81, 134
CYP124	2WM4, 2WM5	*M. tuberculosis*	Fatty acid ω-hydroxylase	Unpublished
CYP125	3IW0-2	*M. tuberculosis*	Cholesterol hydroxylase	82
CYP130	2WH8, 2WHF,2WGY, 2UUQ, 2UVN	*M. tuberculosis*	Ketoconazole inhibited	94
CYP154A1	1ODO	*S. coelicolor*	Unknown	101
CYP154C1	1GWI	*S. coelicolor*	Macrolide	102
CYP158A1	2NZ5, 2NZA, 2DKK	*S. coelicolor*	Flaviolin coupling	173
CYP158A2	2D09, 2D0E, 1SE6, 1T93, 1S1F	*S. coelicolor*	Flaviolin coupling	172
CYP170A1	3DBG	*S. coelicolor*	Albaflavinone	174
CYP175A1	1N97	*T. thermophilus*		159
CYP199A2	2FR7	*Rhodopseudomonas*	p-Subst. benzoic acid	8
CYP231A2	2RFB-C	*Picrophilus (archeon)*		41
CYP245A1 (StaP)	3A1L, 2Z3T-U	*Streptomyces*	Chromopyrrolic acid	74, 148
CYP46A1	2Q9F, 2Q9G	*H. sapiens*	Cholesterol 24-hydroxylase	79
CYP51	2WO9, 2WOA, 2WOB. 1X8V, 1U13, 1EA1, 1E9X	*M. tuberculosis*	Sterol demethylase	11
CYP51	3G1Q, 2VKU, 2CI0, 2CIB, 2BZ9, 1H5Z	*M. tuberculosis*	Sterol 14-α demethylase	24, 103, 104
CYP51	3G1Q, 3GW9	*T. brucei*	Sterol 14-α demethylase	57
CYP51	3I3K	*H. sapiens*	Lanosterol 14-α demethylase	139
CYP55A1 ($P450_{nor}$)	1XQD, 1ULW, 1JFB-C, 1GEJ-K, 1GEI, 1GEM, 1GED. 1CL6, 1CMJ, 1ROM,2ROM,1CMN	*F. oxysporum*	Nitric oxide reductase	53, 96, 136, 137

(*continued*)

Table 1. (Continued)

Enzyme	*Protein Data Base Entries*	*Organism*	*Substrate/Product (if known)*	*References*
CYP74A	2RCH, 2RCL, 2RCM, 3CLI, 3DSI-K	*A. thaliana*	Allene oxide synthase	55, 65
CYP74A2	3DAN,3DBM	*Rubber plant*	Allene oxide synthase	65
CYP1A2	2HI4	*H. sapiens*	Multiple substs.	126
CYP19A1	3I3K	*H. sapiens*	Androgen (aromatase)	29
CYP2A6	3EBS, 2PG5-7, 2FDU-W, 2FDY, 1Z10-1	*H. sapiens*	Multiple substs.	21, 160, 161
CYP2A13	2P85	*H. sapiens*	Multiple substs.	138
CYP2B4	3G5N, 3G93, 2Q6N, 2BDM, 1SUO, 1PO5	*Rabbit*	Multiple substs.	28, 131, 175, 176
CYP2C5	1NR6, 1N6B, 1DT6	*Rabbit*	Multiple substs.	47, 151, 152, 155
CYP2C8	2VN0, 2NNH-J, 1PQ2	*H. sapiens*	Multiple substs.	130
CYP2C9	1R90, 1OG2, 1OG5,	*H. sapiens*	Multiple substs.	153
CYP2D6	2F9Q	*H. sapiens*	Multiple substs.	123
CYP2E1	3E6I, 3E4E	*H. sapiens*	Multiple substs.	105
CYP2R1	3CZH, 3DL9, 3C6G	*H. sapiens*	Vitamin D	140
CYP3A4	2V0M, 2J0D, 1TQN, 1W0E-G	*H. sapiens*	Multiple substs.	25
CYP7A1	3DAX	*H. sapiens*	Cholesterol 7-α-hydroxylase	Unpublished
CYP8A1	3B6H, 2IAG	*H. sapiens*	Prostaglandin I2 (prostacyclin synthase)	68
CYP8A1	3B98, 3B99	*Zebrafish*	Prostaglandin I2 (prostacyclin synthase)	68
XplA	2WIV, 2WIY	*Rhodococcus*	Reductive degradation of RDX	125
P450 EpoK	1Q5D-E	*Sorangium cellulosum*	Epothilone C/A	87
P450 OxyB	1LFK, 1LG9, 1LGF	*Amycolatopsis*	Vancomycin biosynthesis	167
P450 OxyC	1UED	*Amycolatopsis*	Vancomycin biosynthesis	112
P450 BSb	1IZO	*B. subtilis*	Fatty acid oxidation	56
CYPBioI	3EJD, 3EJE3	*E. coli*	Biotin synthesis	15
Thermophilic P450	1UE8	*S. tokodaii*	Unknown	90

a bend in the chain in order to generate precursors for biotin synthesis in *B. subtilis* (15). While CYPBioI does not contain the hϕ-Pro motif at the N-terminal of the B′ helix, the enzyme was crystallized with acyl carrier protein (ACP) bound so as to deliver the bound fatty acid to the active site. The ACP is bound adjacent to the F–G loop and B helix, and is appropriately positioned to force closure of the active site.

In Figure 18, residues involved in the proposed correlations are highlighted in a series of P450 sequences that align with CYP101, but are otherwise uncharacterized. Based on the close alignment, it is expected that, like CYP101, these enzymes catalyze the oxidation of small terpenoids. (CYP101 catalyzes the 5-*exo* hydroxylation of camphor, a small bicyclic terpene). In all of these sequences, the hφ-Pro motif is present at the likely N-terminal of the B′ helix, suggesting regio- and stereospecificity in the chemistry catalyzed. On the I helix, bulky residues are present corresponding to Leu 244 and Val 247 in CYP101, although the Gln and Asn residues in *Proteobacteria* and *S. wittichii* aligned with Leu 244 in the CYP101 sequence may well be removed from the active site. All of the sequences have bulky hydrophobic residues aligned with Val 295 on the β3 strand in CYP101, a primary contact for bound camphor, indicating binding of substrate deep in the active site, these residues being four away from the conserved Arg (Arg 299 in CYP101). Finally, all five sequences have a β-branched hydrophobic side chain (either Val or Leu) aligned with Ile 395, which provides the upper east wall of the active site in CYP101. Of the five sequences, the *S. wittichii* enzyme likely has the least-branched substrate, as the Asn-Phe combination on the I helix could leave an opening adjacent to the I helix to accommodate parts of substrate remote from the site of activity that is not present in the other sequences, while the larger but less constrained Leu side chain on the β3 strand homologous with Val 295 would discourage bulkier groups from binding deep in the active site.

VII. Conclusions

As the number of available P450 structures grows, along with improved dynamic information from NMR and MS methods, it becomes increasingly important to be able to interpret this sea of information without getting lost in it. In

particular, as "personal genomes" become a tool for diagnostics and prescription, the ability to quickly interpret sequence data in terms of expected P450 activity will be critical for assessing the risks and benefits of a particular medication or chemotherapy for an individual patient (6) (Table 1).

In this review, we have attempted to make use of structural and dynamic information obtained by a variety of experimental methods to make some generalizations about how cytochrome P450 enzymes recognize and bind their substrates. In particular, we asked what common features could be used to limit the substrate search space for orphan P450s and to identify the isozyme most likely to metabolize a given small molecule substrate such as a drug or environmental xenobiotic. We conclude, based on comparisons of known P450 structures and dynamic information gleaned from NMR and mass spectrometry, that features of the I helix, β3 and β5 strands adjacent to the active site (with occasional rarer contributions from the A helix for large substrates) are critical for determining which types of substrates will bind. On the other hand, features of the B–C loop, including the B′ helix, and F–G loop are important for determining the final orientation of the bound substrate in the active site, and must reorganize prior to the enzyme reaching a catalytically competent conformation, but are less important for initial substrate binding.

Acknowledgments

This work was supported in part by a grant from the USPHS, R01-GM44191 (TCP). The authors thank Professor Susan Sondej Pochapsky for her critical reading of the manuscript, and all of the reviewers for helpful suggestions.

References

1. Aldag C, Gromov IA, Garcia–Rubio I, von Koenig K, Schlichting I, Jaun B, and Hilvert D. Probing the role of the proximal heme ligand in cytochrome P450cam by recombinant incorporation of selenocysteine. *Proc Natl Acad Sci USA* 106: 5481–5486, 2009.
2. Altschul SF, Madden TL, Schaffer AA, Zhang JH, Zhang Z, Miller W, and Lipman DJ. Gapped BLAST and PSI-BLAST: A new generation of protein database search programs. *Nucleic Acids Res* 25: 3389–3402, 1997.
3. Andersen JF, Tatsuta K, Gunji H, Ishiyama T, and Hutchinson CR. Substrate-apecificity of 6-Deoxyerythronolide-B hydroxylase, a bacterial cytochrome P450 of erythromycin-a biosynthesis. *Biochemistry* 32: 1905–1913, 1993.
4. Arimoto R. Computational models for predicting interactions with cytochrome P450 enzyme. *Current Topics Med Chem* 6: 1609–1618, 2006.
5. Asciutto EK, Madura JD, Pochapsky SS, OuYang B, and Pochapsky TC. Structural and dynamic implications of an effector-induced backbone amide cis-trans isomerization in cytochrome P450(cam). *J Mol Biol* 388: 801–814, 2009.
6. Bai JPF. Ongoing challenges in drug interaction safety: From exposure to pharmacogenomics. *Drug Metab Pharmacokin* 25: 62–71, 2010.
7. Belin P, Le Du MH, Fielding A, Lequin O, Jacquet M, Charbonnier JB, Lecoq A, Thai R, Courcon M, Masson C, Dugave C, Genet R, Pernodet JL, and Gondry M. Identification and structural basis of the reaction catalyzed by CYP121, an essential cytochrome P450 in *Mycobacterium tuberculosis*. *Proc Natl Acad Sci USA* 106: 7426–7431, 2009.
8. Bell SG, Xu F, Forward I, Bartlam M, Rao Z, and Wong LL. Crystal structure of CYP199A2, a para-substituted benzoic acid oxidizing cytochrome P450 from *Rhodopseudomonas palustris*. *J Mol Biol* 383: 561–574, 2008.
9. Blake CCF, Koenig DF, Mair GA, North ACT, Phillips DC, and Sarma VR. Structure of hen egg-white lysozyme: A 3-dimensional fourier Ssynthesis at 2 Å resolution. *Nature* 206: 757, 1965.
10. Cameron MD, Wen B, Allen KE, Roberts AG, Schuman JT, Campbell AP, Kunze KL, and Nelson SD. Cooperative binding of midazolam with testosterone and alpha-naphthoflavone within the CYP3A4 active site: A NMR T-1 paramagnetic relaxation study. *Biochemistry* 44: 14143–14151, 2005.
11. Chen CK, Doyle PS, Yermalitskaya LV, Mackey ZB, Ang KK, McKerrow JH, and Podust LM. *Trypanosoma cruzi* CYP51 inhibitor derived from a *Mycobacterium tuberculosis* screen hit. *PLoS Negl Trop Dis* 3: e372, 2009.
12. Chen LM, Brugger K, Skovgaard M, Redder P, She QX, Torarinsson E, Greve B, Awayez M, Zibat A, Klenk HP, and Garrett RA. The genome of *Sulfolobus acidocaldarius*, a model organism of the Crenarchaeota. *J Bacteriol* 187: 4992–4999, 2005.
13. Chen S and Zhou DJ. Functional domains of aromatase cytochrome-P450 inferred from comparative analyses of amino acid sequences and substantiated by site-directed mutagenesis Eexperiments. *J Biol Chem* 267: 22587–22594, 1992.
14. Clark JP, Miles CS, Mowat CG, Walkinshaw MD, Reid GA, Daff SN, and Chapman SK. The role of Thr268 and Phe393 in cytochrome P450 BM3. *J Inorg Biochem* 100: 1075–1090, 2006.
15. Cryle MJ and Schlichting I. Structural insights from a P450 Carrier Protein complex reveal how specificity is achieved in the P450(BioI) ACP complex. *Proc Natl Acad Sci USA* 105: 15696–15701, 2008.
16. Cupp–Vickery J, Anderson R, and Hatziris Z. Crystal structures of ligand complexes of P450eryF exhibiting homotropic cooperativity. *Proc Natl Acad Sci USA* 97: 3050–3055, 2000.
17. Cupp–Vickery JR, Garcia C, Hofacre A, and McGee–Estrada K. Ketoconazole-induced conformational changes in the active site of cytochrome P450eryF. *J Mol Biol* 311: 101–110, 2001.
18. Cupp–Vickery JR and Poulos TL. Structure of cytochrome P450eryF involved in erythromycin biosynthesis. *Nat Struct Biol* 2: 144–153, 1995.
19. de Graaf C, Oostenbrink C, Keizers PHJ, van Vugt-Lussenburg BMA, van Waterschoot RAB, Tschirret-Guth RA, Commandeur JNM, and Vermeulen NPE. Molecular modeling-guided site-directed mutagenesis of cytochrome P450 2D6. *Current Drug Metabolism* 8: 59–77, 2007.
20. DeLano WL. The PyMOL Molecular Graphics System. 2008.
21. DeVore NM, Smith BD, Urban MJ, and Scott EE. Key residues controlling phenacetin metabolism by human cytochrome P450 2A enzymes. *Drug Metab Dispos* 36: 2582–2590, 2008.
22. Dmochowski IJ, Crane BR, Wilker JJ, Winkler JR, and Gray HB. Optical detection of cytochrome P450 by sensitizer-linked substrates. *Proc Natl Acad Sci USA* 96: 12987–12990, 1999.
23. Dunn AR, Dmochowski IJ, Bilwes AM, Gray HB, and Crane BR. Probing the open state of cytochrome P450cam with ruthenium-linker substrates. *Proc Natl Acad Sci USA* 98: 12420–12425, 2001.

24. Eddine AN, von Kries JP, Podust MV, Warrier T, Kaufmann SH, and Podust LM. X-ray structure of 4,4′-dihydroxybenzophenone mimicking sterol substrate in the active site of sterol 14alpha-demethylase (CYP51). *J Biol Chem* 283: 15152–15159, 2008.
25. Ekroos M and Sjogren T. Structural basis for ligand promiscuity in cytochrome P450 3A4. *Proc Natl Acad Sci USA* 103: 13682–13687, 2006.
26. Fedorov R, Ghosh DK, and Schlichting I. Crystal structures of cyanide complexes of P450cam and the oxygenase domain of inducible nitric oxide synthase-structural models of the short-lived oxygen complexes. *Arch Biochem Biophys* 409: 25–31, 2003.
27. Fruetel JA, Mackman RL, Peterson JA, and Ortiz de Montellano PR. Relationship of active site topology to substrate specificity for cytochrome P450terp (CYP108). *J Biol Chem* 269: 28815–28821, 1994.
28. Gay SC, Sun L, Maekawa K, Halpert JR, and Stout CD. Crystal structures of cytochrome P450 2B4 in complex with the inhibitor 1-biphenyl-4-methyl-1H-imidazole: Ligand-induced structural response through alpha-helical repositioning. *Biochemistry* 48: 4762–4771, 2009.
29. Ghosh D, Griswold J, Erman M, and Pangborn W. Structural basis for androgen specificity and oestrogen synthesis in human aromatase. *Nature* 457: 219–U119, 2009.
30. Girvan HM, Seward HE, Toogood HS, Cheesman MR, Leys D, and Munro AW. Structural and spectroscopic characterization of P450 BM3 mutants with unprecedented P450 heme iron ligand sets. New heme ligation states influence conformational equilibria in P450 BM3. *J Biol Chem* 282: 564–572, 2007.
31. Girvan HM, Toogood HS, Littleford RE, Seward HE, Smith WE, Ekanem IS, Leys D, Cheesman MR, and Munro AW. Novel haem co-ordination variants of flavocytochrome P450BM3. *Biochem J* 417: 65–76, 2009.
32. Gotoh O. Substrate recognition sites in cytochrome-P450 family-2 (CYP2) proteins inferred from comparative analyses of amino acid and coding nucleotide sequences. *J Biol Chem* 267: 83–90, 1992.
33. Haines DC, Chen B, Tomchick DR, Bondlela M, Hegde A, Machius M, and Peterson JA. Crystal structure of inhibitor-bound P450BM-3 reveals open conformation of substrate access channel. *Biochemistry* 47: 3662–3670, 2008.
34. Haines DC, Tomchick DR, Machius M, and Peterson JA. Pivotal role of water in the mechanism of P450BM-3. *Biochemistry* 40: 13456–13465, 2001.
35. Hamuro Y, Molnar KS, Coales SJ, OuYang B, Simorellis AK, and Pochapsky TC. Hydrogen-deuterium exchange mass spectrometry for investigation of backbone dynamics of oxidized and reduced cytochrome P450(cam). *J Inorg Biochem* 102: 364–370, 2008.
36. Hannemann F, Bichet A, Ewen KM, and Bernhardt R. Cytochrome P450 systems. Biological variations of electron transport chains. *Biochim Biophys Acta-Gen Subj* 1770: 330–344, 2007.
37. Hasemann CA, Ravichandran KG, Peterson JA, and Deisenhofer J. Crystal structure and refinement of cytochrome P450terp at 2.3 A resolution. *J Mol Biol* 236: 1169–1185, 1994.
38. Hayashi K, Sugimoto H, Shinkyo R, Yamada M, Ikeda S, Ikushiro S, Kamakura M, Shiro Y, and Sakaki T. Structure-based design of a highly active vitamin D hydroxylase from *Streptomyces griseolus* CYP105A1. *Biochemistry* 47: 11964–11972, 2008.
39. Hegde A, Haines DC, Bondlela M, Chen B, Schaffer N, Tomchick DR, Machius M, Nguyen H, Chowdhary PK, Stewart L, Lopez C, and Peterson JA. Interactions of substrates at the surface of P450s can greatly enhance substrate potency. *Biochemistry* 46: 14010–14017, 2007.
40. Hlavica P. Functional interaction of nitrogenous organic bases with cytochrome P450: A critical assessment and update of substrate features and predicted key active-site elements steering the access, binding, and orientation of amines. *Biochim Biophys Acta-Proteins Proteomics* 1764: 645–670, 2006.
41. Ho WW, Li H, Nishida CR, de Montellano PR, and Poulos TL. Crystal structure and properties of CYP231A2 from the thermoacidophilic archaeon *Picrophilus torridus. Biochemistry* 47: 2071–2079, 2008.
42. Hsu MH, Griffin KJ, Wang Y, Kemper B, and Johnson EF. A single amino acid substitution confers progesterone 6-beta-hydroxylase activity to rabbit cytochrome P450 2C3. *J Biol Chem* 268: 6939–6944, 1993.
43. Huang WC, Westlake AC, Marechal JD, Joyce MG, Moody PC, and Roberts GC. Filling a hole in cytochrome P450 BM3 improves substrate binding and catalytic efficiency. *J Mol Biol* 373: 633–651, 2007.
44. Hummel MA, Gannett PM, Aguilar J, and Tracy TS. Substrate proton to heme distances in CYP2C9 allelic variants and alterations by the heterotropic activator, dapsone. *Arch Biochem Biophys* 475: 175–183, 2008.
45. Hutter MC. In silico prediction of drug properties. *Curr Med Chem*16: 189–202, 2009.
46. Iwasaki M, Darden TA, Pedersen LG, Davis DG, Juvonen RO, Sueyoshi T, and Negishi M. Engineering mouse P450coh to a novel corticosterone 15-alpha-hydroxylase and modeling steroid-binding orientation in the substrate pocket. *J Biol Chem* 268: 759–762, 1993.
47. Johnson EF, Wester MR, and Stout CD. The structure of microsomal cytochrome P450 2C5: A steroid and drug metabolizing enzyme. *Endocrine Res* 28: 435–441, 2002.
48. Jovanovic T, Harris M, and McDermott AE. Cytochrome P450BM-3 in complex with its substrate: Temperature-dependent spin state equilibria in the oxidized and reduced states. *Applied Magnetic Resonance* 31: 411–429, 2007.
49. Jovanovic T and McDermott AE. Observation of ligand binding to cytochrome P450 BM-3 by means of solid-state NMR spectroscopy. *J Am Chem Soc* 127: 13816–13821, 2005.
50. Kendrew JC, Bodo G, Dintzis HM, Parrish RG, Wyckoff H, and Phillips DC. 3-dimensional model of the myoglobin molecule obtained by X-ray analysis. *Nature* 181: 662–666, 1958.
51. Kijac AZ, Li Y, Sligar SG, and Rienstra CM. Magic-angle spinning solid-state NMR Spectroscopy of nanodisc-embedded human CYP3A4. *Biochemistry* 46: 13696–13703, 2007.
52. Koo LS, Immoos CE, Cohen MS, Farmer PJ, and de Montellano PRO. Enhanced electron transfer and lauric acid hydroxylation by site-directed mutagenesis of CYP119. *J Am Chem Soc* 124: 5684–5691, 2002.
53. Kudo T, Takaya N, Park SY, Shiro Y, and Shoun H. A positively charged cluster formed in the heme-distal pocket of cytochrome P450nor is essential for interaction with NADH. *J Biol Chem* 276: 5020–5026, 2001.
54. Kuhnel K, Ke N, Cryle MJ, Sligar SG, Schuler MA, and Schlichting I. Crystal structures of substrate-free and retinoic acid-bound cyanobacterial cytochrome P450 CYP120A1. *Biochemistry* 31: 31, 2008.

55. Lee DS, Nioche P, Hamberg M, and Raman CS. Structural insights into the evolutionary paths of oxylipin biosynthetic enzymes. *Nature* 455: 363–368, 2008.
56. Lee DS, Yamada A, Sugimoto H, Matsunaga I, Ogura H, Ichihara K, Adachi S, Park SY, and Shiro Y. Substrate recognition and molecular mechanism of fatty acid hydroxylation by cytochrome P450 from *Bacillus subtilis*. Crystallographic, spectroscopic, and mutational studies. *J Biol Chem* 278: 9761–9767, 2003.
57. Lepesheva GI, Park HW, Hargrove TY, Vanhollebeke B, Wawrzak Z, Chaudhuri M, Villalta F, and Waterman MR. Crystal structures of *Trypanosoma brucei* sterol 14 alpha-demethylase and implications for selective treatment of human infections *J Biol Chem* 285: 1773–1780, 2010.
58. Lepesheva GI, Virus C, and Waterman MR. Conservation in the CYP51 family. Role of the B ′ helix/BC loop and helices F and G in enzymatic function. *Biochemistry* 42: 9091–9101, 2003.
59. Lewis DFV and Ito Y. Human P450s involved in drug metabolism and the use of structural modelling for understanding substrate selectivity and binding affinity. *Xenobiotica* 39: 625–635, 2009.
60. Lewis DFV, Ito Y, and Goldfarb PS. Investigating human P450s involved in drug metabolism via homology with high-resolution P450 crystal structures of the CYP2C subfamily. *Curr Drug Metab* 7: 589–598, 2006.
61. Lewis DFV, Ito Y, and Goldfarb PS. Structural modelling of the human drug-metabolizing cytochromes P450. *Curr Med Chem* 13: 2645–2652, 2006.
62. Leys D, Mowat CG, McLean KJ, Richmond A, Chapman SK, Walkinshaw MD, and Munro AW. Atomic structure of *Mycobacterium tuberculosis* CYP121 to 1.06 Å reveals novel features of cytochrome P450. *J Biol Chem* 278: 5141–5147, 2003.
63. Li H and Poulos TL. Modeling protein-substrate interactions in the heme domain of cytochrome P450(BM-3). *Acta Crystallogr D Biol Crystallogr* 51: 21–32, 1995.
64. Li H and Poulos TL. The structure of the cytochrome P450BM-3 haem domain complexed with the fatty acid substrate, palmitoleic acid. *Nat Struct Biol* 4: 140–146, 1997.
65. Li L, Chang Z, Pan Z, Fu ZQ, and Wang X. Modes of heme binding and substrate access for cytochrome P450 CYP74A revealed by crystal structures of allene oxide synthase. *Proc Natl Acad Sci USA* 105: 13883–13888, 2008.
66. Li S, Ouellet H, Sherman DH, and Podust LM. Analysis of transient and catalytic desosamine-binding pockets in cytochrome P450 PikC from *Streptomyces venezuelae*. *J Biol Chem* 284: 5723–5730, 2009.
67. Li SY, Chaulagain MR, Knauff AR, Podust LM, Montgomery J, and Sherman DH. Selective oxidation of carbolide C-H bonds by an engineered macrolide P450 mono-oxygenase. *Proc Natl Acad Sci USA* 106: 18469–18474, 2009.
68. Li YC, Chiang CW, Yeh HC, Hsu PY, Whitby FG, Wang LH, and Chan NL. Structures of prostacyclin synthase and its complexes with substrate analog and inhibitor reveal a ligand-specific heme conformation change. *J Biol Chem* 283: 2917–2926, 2008.
69. Liao WL, Dodder NG, Mast N, Pikuleva IA, and Turko IV. Steroid and protein ligand binding to cytochrome P450 46A1 as assessed by hydrogen-deuterium exchange and mass spectrometry. *Biochemistry* 48: 4150–4158, 2009.
70. Lipscomb JD, Sligar SG, Namtvedt MJ, and Gunsalus IC. Autooxidation and Hhydroxylation reactions of oxygenated cytochrome P450cam. *J Biol Chem* 251: 1116–1124, 1976.
71. Ludemann SK, Lounnas V, and Wade RC. How do substrates enter and products exit the buried active site of cytochrome P450cam? 1. Random expulsion molecular dynamics investigation of ligand access channels and mechanisms. *J Mol Biol* 303: 797–811, 2000.
72. Ludemann SK, Lounnas V, and Wade RC. How do substrates enter and products exit the buried active site of cytochrome P450cam? 2. Steered molecular dynamics and adiabatic mapping of substrate pathways. *J Mol Biol* 303: 813–830, 2000.
73. Lyons TA, Ratnaswamy G, and Pochapsky TC. Redox-dependent dynamics of putidaredoxin characterized by amide proton exchange. *Protein Science* 5: 627–639, 1996.
74. Makino M, Sugimoto H, Shiro Y, Asamizu S, Onaka H, and Nagano S. Crystal structures and catalytic mechanism of cytochrome P450 StaP that produces the indolocarbazole skeleton. *Proc Natl Acad Sci USA* 104: 11591–11596, 2007.
75. Makris TM, von Koenig K, Schlichting I, and Sligar SG. Alteration of P450 distal pocket solvent leads to impaired proton delivery and changes in heme geometry. *Biochemistry* 46: 14129–14140, 2007.
76. Makris TM, von Koenig K, Schlichting I, and Sligar SG. The status of high-valent metal oxo complexes in the P450 cytochromes. *J Inorg Biochem* 100: 507–518, 2006.
77. Mansuy D. Biocatalysis and substrate chemodiversity: Adaptation of aerobic living organisms to their chemical environment. *Catalysis Today* 138: 2–8, 2008.
78. Mast N, Liao WL, Pikuleva IA, and Turko IV. Combined use of mass spectrometry and heterologous expression for identification of membrane-interacting peptides in cytochrome P450 46A1 and NADPH-cytochrome P450 oxidoreductase. *Arch Biochem Biophys* 483: 81–89, 2009.
79. Mast N, White MA, Bjorkhem I, Johnson EF, Stout CD, and Pikuleva IA. Crystal structures of substrate-bound and substrate-free cytochrome P450 46A1, the principal cholesterol hydroxylase in the brain. *Proc Natl Acad Sci USA* 105: 9546–9551, 2008.
80. McCullough CR, Pullela PK, Im SC, Waskell L, and Sem DS. C-13-methyl isocyanide as an NMR probe for cytochrome P450 active sites. *J Biomol NMR* 43: 171–178, 2009.
81. McLean KJ, Carroll P, Lewis DG, Dunford AJ, Seward HE, Neeli R, Cheesman MR, Marsollier L, Douglas P, Smith WE, Rosenkrands I, Cole ST, Leys D, Parish T, and Munro AW. Characterization of active site structure in CYP121. A cytochrome P450 essential for viability of *Mycobacterium tuberculosis* H37Rv. *J Biol Chem* 283: 33406–33416, 2008.
82. McLean KJ, Lafite P, Levy C, Cheesman MR, Mast N, Pikuleva IA, Leys D, and Munro AW. The structure of *Mycobacterium tuberculosis* CYP125: Molecular basis for cholesterol binding in a P450 needed for host infection. *J Biol Chem* 284: 35524–35533, 2009.
83. Modi S, Paine MJ, Sutcliffe MJ, Lian LY, Primrose WU, Wolf CR, and Roberts GCK. A model for human cytochrome P450 2D6 based on homology modeling and NMR studies of substrate binding. *Biochemistry* 35: 4540–4550, 1996.
84. Modi S, Sutcliffe MJ, Primrose WU, Lian LY, and Roberts GCK. The catalytic mechanism of cytochrome P450 BM3 involves a 6 angstrom movement of the bound substrate on reduction. *Nature Structural Biology* 3: 414–417, 1996.
85. Myers TG, Thummel KE, Kalhorn TF, and Nelson SD. Preferred orientations in the binding of 4′-hydroxyacetanilide (acetaminophen) to cytochrome P450 1A1 and 2B1 isoforms

as determined by C13 NMR and N15 NMR relaxation studies. *J Med Chem* 37: 860–867, 1994.
86. Nagano S, Cupp–Vickery JR, and Poulos TL. Crystal structures of the ferrous dioxygen complex of wild-type cytochrome P450eryF and its mutants, A245S and A245T: investigation of the proton transfer system in P450eryF. *J Biol Chem* 280: 22102–22107, 2005.
87. Nagano S, Li H, Shimizu H, Nishida C, Ogura H, Ortiz de Montellano PR, and Poulos TL. Crystal structures of epothilone D-bound, epothilone B-bound, and substrate-free forms of cytochrome P450epoK. *J Biol Chem* 278: 44886–44893, 2003.
88. Nagano S and Poulos TL. Crystallographic study on the dioxygen complex of wild-type and mutant cytochrome P450cam. Implications for the dioxygen activation mechanism. *J Biol Chem* 280: 31659–31663, 2005.
89. Nagano S, Tosha T, Ishimori K, Morishima I, and Poulos TL. Crystal structure of the cytochrome P450cam mutant that exhibits the same spectral perturbations induced by putidaredoxin binding. *J Biol Chem* 279: 42844–42849, 2004.
90. Oku Y, Ohtaki A, Kamitori S, Nakamura N, Yohda M, Ohno H, and Kawarabayasi Y. Structure and direct electrochemistry of cytochrome P450 from the thermoacidophilic crenarchaeon, *Sulfolobus tokodaii* strain 7. *J Inorg Biochem* 98: 1194–1199, 2004.
91. Oshima R, Fushinobu S, Su F, Zhang L, Takaya N, and Shoun H. Structural evidence for direct hydride transfer from NADH to cytochrome P450nor. *J Mol Biol* 342: 207–217, 2004.
92. Ost TW, Clark J, Mowat CG, Miles CS, Walkinshaw MD, Reid GA, Chapman SK, and Daff S. Oxygen activation and electron transfer in flavocytochrome P450 BM3. *J Am Chem Soc* 125: 15010–15020, 2003.
93. Ost TW, Munro AW, Mowat CG, Taylor PR, Pesseguiero A, Fulco AJ, Cho AK, Cheesman MA, Walkinshaw MD, and Chapman SK. Structural and spectroscopic analysis of the F393H mutant of flavocytochrome P450 BM3. *Biochemistry* 40: 13430–13438, 2001.
94. Ouellet H, Podust LM, and de Montellano PR. *Mycobacterium tuberculosis* CYP130: crystal structure, biophysical characterization, and interactions with antifungal azole drugs. *J Biol Chem* 283: 5069–5080, 2008.
95. OuYang B, Pochapsky SS, Dang M, and Pochapsky TC. A functional proline switch in cytochrome P450(cam). *Structure* 16: 916–923, 2008.
96. Park SY, Shimizu H, Adachi S, Nakagawa A, Tanaka I, Nakahara K, Shoun H, Obayashi E, Nakamura H, Iizuka T, and Shiro Y. Crystal structure of nitric oxide reductase from denitrifying fungus Fusarium oxysporum. *Nat Struct Biol* 4: 827–832, 1997.
97. Park SY, Yamane K, Adachi S, Shiro Y, Weiss KE, Maves SA, and Sligar SG. Thermophilic cytochrome P450 (CYP119) from *Sulfolobus solfataricus*: high resolution structure and functional properties. *J Inorg Biochem* 91: 491–501, 2002.
98. Pochapsky SS, Dang M, OuYang B, Simorellis AK, and Pochapsky TC. Redox-dependent dynamics in cytochrome P450(cam). *Biochemistry* 48: 4254-4261, 2009.
99. Pochapsky SS, Pochapsky TC, and Wei JW. A model for effector activity in a highly specific biological electron transfer complex: The cytochrome P450(cam)-putidaredoxin couple. *Biochemistry* 42: 5649–5656, 2003.
100. Pochapsky TC, Lyons TA, Kazanis S, Arakaki T, and Ratnaswamy G. A structure-based model for cytochrome P450(cam)-putidaredoxin interactions. *Biochimie* 78: 723–733, 1996.
101. Podust LM, Bach H, Kim Y, Lamb DC, Arase M, Sherman DH, Kelly SL, Waterman MR, Schoch GA, Yano JK, Wester MR, Griffin KJ, Stout CD, and Johnson EF. Comparison of the 1.85 Å structure of CYP154A1 from *Streptomyces coelicolor* A3(2) with the closely related CYP154C1 and CYPs from antibiotic biosynthetic pathways. *Protein Sci* 13: 255–268, 2004.
102. Podust LM, Kim Y, Arase M, Neely BA, Beck BJ, Bach H, Sherman DH, Lamb DC, Kelly SL, and Waterman MR. The 1.92-A structure of *Streptomyces coelicolor* A3(2) CYP154C1. A new monooxygenase that functionalizes macrolide ring systems. *J Biol Chem* 278: 12214–12221, 2003.
103. Podust LM, Poulos TL, and Waterman MR. Crystal structure of cytochrome P450 14-alpha-sterol demethylase (CYP51) from *Mycobacterium tuberculosis* in complex with azole inhibitors. *Proc Natl Acad Sci USA* 98: 3068–3073, 2001.
104. Podust LM, von Kries JP, Eddine AN, Kim Y, Yermalitskaya LV, Kuehne R, Ouellet H, Warrier T, Altekoster M, Lee JS, Rademann J, Oschkinat H, Kaufmann SH, and Waterman MR. Small-molecule scaffolds for CYP51 inhibitors identified by high-throughput screening and defined by X-ray crystallography. *Antimicrob Agents Chemother* 51: 3915–3923, 2007.
105. Porubsky PR, Meneely KM, and Scott EE. Structures of human cytochrome P450 2E1. Insights into the binding of inhibitors and both small molecular weight and fatty acid substrates. *J Biol Chem* 283: 33698–33707, 2008.
106. Poulos TL. Modeling of mammalian P450s on basis of P450cam X-ray structure. *Methods Enzymol* 206: 11–30, 1991.
107. Poulos TL. Structural biology of P450-oxy complexes. *Drug Metab Rev* 39: 557–566, 2007.
108. Poulos TL, Finzel BC, and Howard AJ. Crystal structure of substrate-free *Pseudomonas putida* cytochrome P450. *Biochemistry* 25: 5314–5322, 1986.
109. Poulos TL, Finzel BC, and Howard AJ. High-resolution crystal structure of cytochrome P450cam. *J Mol Biol* 195: 687–700, 1987.
110. Poulos TL and Howard AJ. Crystal structures of metyrapone- and phenylimidazole-inhibited complexes of cytochrome P450cam. *Biochemistry* 26: 8165–8174, 1987.
111. Prusis P and Afzelius L. Improvement of site of metabolism predictions for CYP3A4 by using discriminant analysis of compound preference of CYP3A4 X-ray structural conformers and subsequent docking. *QSAR Comb Sci* 28: 865–868, 2009.
112. Pylypenko O, Vitali F, Zerbe K, Robinson JA, and Schlichting I. Crystal structure of OxyC, a cytochrome P450 implicated in an oxidative C-C coupling reaction during vancomycin biosynthesis. *J Biol Chem* 278: 46727–46733, 2003.
113. Raag R, Li H, Jones BC, and Poulos TL. Inhibitor-induced conformational change in cytochrome P450CAM. *Biochemistry* 32: 4571–4578, 1993.
114. Raag R, Martinis SA, Sligar SG, and Poulos TL. Crystal structure of the cytochrome P450cam active site mutant Thr252Ala. *Biochemistry* 30: 11420–11429, 1991.
115. Raag R and Poulos TL. Crystal structure of the carbon monoxide-substrate-cytochrome P450CAM ternary complex. *Biochemistry* 28: 7586–7592, 1989.
116. Raag R and Poulos TL. Crystal structures of cytochrome P450cam complexed with camphane, thiocamphor, and adamantane: Factors controlling P450 substrate hydroxylation. *Biochemistry* 30: 2674–2684, 1991.
117. Raag R and Poulos TL. The structural basis for substrate-induced changes in redox potential and spin equilibrium in cytochrome P450CAM. *Biochemistry* 28: 917–922, 1989.

118. Raag R, Swanson BA, Poulos TL, and Ortiz de Montellano PR. Formation, crystal structure, and rearrangement of a cytochrome P450cam iron–phenyl complex. *Biochemistry* 29: 8119–8126, 1990.
119. Ravichandran KG, Boddupalli SS, Hasermann CA, Peterson JA, and Deisenhofer J. Crystal structure of hemoprotein domain of P450BM-3, a prototype for microsomal P450's. *Science* 261: 731–736, 1993.
120. Roberts AG, Diaz MD, Lampe JN, Shireman LM, Grinstead JS, Dabrowski MJ, Pearson JT, Bowman MK, Atkins WM, and Campbell AP. NMR studies of ligand binding to P450(ery)F provides insight into the mechanism of cooperativity. *Biochemistry* 45: 1673–1684, 2006.
121. Roberts ES, Ballou DP, Hopkins NE, Alworth WL, and Hollenberg PF. Mechanistic Studies of 9-Ethynylphenanthrene-Inactivated Cytochrome-P450 2b1. *Arch Biochem Biophys* 323: 303–312, 1995.
122. Roberts GCK, Sutcliffe MJ, Modi S, Lian LY, Primrose WU, and Wolf CR. Construction of models of P450-substrate complexes by a combination of NMR and homology modelling. *FASEB J* 11: A778–A778, 1997.
123. Rowland P, Blaney FE, Smyth MG, Jones JJ, Leydon VR, Oxbrow AK, Lewis CJ, Tennant MG, Modi S, Eggleston DS, Chenery RJ, and Bridges AM. Crystal structure of human cytochrome P450 2D6. *J Biol Chem* 281: 7614–7622, 2006.
124. Rupasinghe SG, Duan H, Schmidt HLF, Berthold DA, Rienstra CM, and Schuler MA. High-yield expression and purification of isotopically labeled cytochrome P450 monooxygenases for solid-state NMR spectroscopy. *Biochim Biophys Acta-Biomembranes* 1768: 3061–3070, 2007.
125. Sabbadin F, Jackson R, Haider K, Tampi G, Turkenburg JP, Hart S, Bruce NC, and Grogan G. The 1.5 A structure of XplA-heme, an unusual cytochrome-P450 heme domain that catalyses reductive biotransformation of royal demolition explosive (RDX). *J Biol Chem* 284: 28467–28475, 2009.
126. Sansen S, Yano JK, Reynald RL, Schoch GA, Griffin KJ, Stout CD, and Johnson EF. Adaptations for the oxidation of polycyclic aromatic hydrocarbons exhibited by the structure of human P450 1A2. *J Biol Chem* 282: 14348–14355, 2007.
127. Savino C, Montemiglio LC, Sciara G, Miele AE, Kendrew SG, Jemth P, Gianni S, and Vallone B. Investigating the structural plasticity of a cytochrome P450: Three dimensional structures of P450 EryK and binding to its physiological substrate. *J Biol Chem* 284: 291700–29179, 2009.
128. Schlichting I, Berendzen J, Chu K, Stock AM, Maves SA, Benson DE, Sweet RM, Ringe D, Petsko GA, and Sligar SG. The catalytic pathway of cytochrome P450cam at atomic resolution. *Science* 287: 1615–1622, 2000.
129. Schlichting I, Jung C, and Schulze H. Crystal structure of cytochrome P450cam complexed with the (1S)-camphor enantiomer. *FEBS Lett* 415: 253–257, 1997.
130. Schoch GA, Yano JK, Sansen S, Dansette PM, Stout CD, and Johnson EF. Determinants of cytochrome P450 2C8 substrate binding: Structures of complexes with montelukast, troglitazone, felodipine, and 9-cis-retinoic acid. *J Biol Chem* 283: 17227–17237, 2008.
131. Scott EE, He YA, Wester MR, White MA, Chin CC, Halpert JR, Johnson EF, and Stout CD. An open conformation of mammalian cytochrome P450 2B4 at 1.6-Å resolution. *Proc Natl Acad Sci USA* 100: 13196–13201, 2003.
132. Scott EE, White MA, He YA, Johnson EF, Stout CD, and Halpert JR. Structure of mammalian cytochrome P4502B4 complexed with 4-(4-chlorophenyl) imidazole at 1.9-angstrom resolution. Insight into the range of P450 conformations and the coordination of redox partner binding. *J Biol Chem* 279: 27294–27301, 2004.
133. Sevrioukova IF, Li H, Zhang H, Peterson JA, and Poulos TL. Structure of a cytochrome P450-redox partner electron-transfer complex. *Proc Natl Acad Sci USA* 96: 1863–1868, 1999.
134. Seward HE, Roujeinikova A, McLean KJ, Munro AW, and Leys D. Crystal structure of the *Mycobacterium tuberculosis* P450 CYP121-fluconazole complex reveals new azole drug-P450 binding mode. *J Biol Chem* 281: 39437–39443, 2006.
135. Sherman DH, Li S, Yermalitskaya LV, Kim Y, Smith JA, Waterman MR, and Podust LM. The structural basis for substrate anchoring, active site selectivity, and product formation by P450 PikC from *Streptomyces venezuelae*. *J Biol Chem* 281: 26289–26297, 2006.
136. Shimizu H, Obayashi E, Gomi Y, Arakawa H, Park SY, Nakamura H, Adachi S, Shoun H, and Shiro Y. Proton delivery in NO reduction by fungal nitric-oxide reductase. Cryogenic crystallography, spectroscopy, and kinetics of ferric-NO complexes of wild-type and mutant enzymes. *J Biol Chem* 275: 4816–4826, 2000.
137. Shimizu H, Park SY, Shiro Y, and Adachi S. X-ray structure of nitric oxide reductase (cytochrome P450nor) at atomic resolution. *Acta Crystallogr D Biol Crystallogr* 58: 81–89, 2002.
138. Smith BD, Sanders JL, Porubsky PR, Lushington GH, Stout CD, and Scott EE. Structure of the human lung cytochrome P450 2A13. *J Biol Chem* 282: 17306–17313, 2007.
139. Strushkevich N, Usanov SA, and Park H–W. Structural basis of human CYP51 inhibition by antifungal azoles. *J Mol Biol* 397: 1067–1078, 2010.
140. Strushkevich N, Usanov SA, Plotnikov AN, Jones G, and Park HW. Structural analysis of CYP2R1 in complex with vitamin D3. *J Mol Biol* 380: 95–106, 2008.
141. Sugimoto H, Shinkyo R, Hayashi K, Yoneda S, Yamada M, Kamakura M, Ikushiro S, Shiro Y, and Sakaki T. Crystal structure of CYP105A1 (P450SU-1) in complex with 1alpha, 25-dihydroxyvitamin D3. *Biochemistry* 47: 4017–4027, 2008.
142. Tosha T, Yoshioka S, Ishimori K, and Morishima I. L358P mutation on cytochrome P450cam simulates structural changes upon putidaredoxin binding. The structural changes trigger electron transfer to oxy-P450cam from electron donors. *J Biol Chem* 279: 42836–42843, 2004.
143. Tosha T, Yoshioka S, Takahashi S, Ishimori K, Shimada H, and Morishima I. NMR study on the structural changes of cytochrome P450cam upon the complex formation with putidaredoxin. Functional significance of the putidaredoxin-induced structural changes. *J Biol Chem* 278: 39809–39821, 2003.
144. Verras A, Alian A, and de Montellano PR. Cytochrome P450 active site plasticity: attenuation of imidazole binding in cytochrome P450(cam) by an L244A mutation. *Protein Eng Des Sel* 19: 491–496, 2006.
145. Vidakovic M, Sligar SG, Li H, and Poulos TL. Understanding the role of the essential Asp251 in cytochrome P450cam using site-directed mutagenesis, crystallography, and kinetic solvent isotope effect. *Biochemistry* 37: 9211–9219, 1998.
146. vonWachenfeldt C, Richardson TH, Cosme J, and Johnson EF. Microsomal P450 2C3 is expressed as a soluble dimer in *Escherichia coli* following modifications of its N-terminus. *Arch Biochem Biophys* 339: 107–114, 1997.
147. Wang B and Zhou SF. Synthetic and natural compounds that interact with human cytochrome P450 1A2 and implications in drug development. *Curr Med Chem* 16: 4066–4218, 2009.

148. Wang Y, Chen H, Makino M, Shiro Y, Nagano S, Asamizu S, Onaka H, and Shaik S. Theoretical and experimental studies of the conversion of chromopyrrolic acid to an antitumor derivative by cytochrome P450 StaP: The catalytic role of water molecules. *J Am Chem Soc* 131: 6748–6762, 2009.
149. Wei JY, Pochapsky TC, and Pochapsky SS. Detection of a high-barrier conformational change in the active site of cytochrome P450(cam) upon binding of putidaredoxin. *J Am Chem Soc* 127: 6974–6976, 2005.
150. Wen B, Doneanu CE, Gartner CA, Roberts AG, Atkins WM, and Nelson SD. Fluorescent photoaffinity labeling of cytochrome P450 3A4 by lapachenole: Identification of modification sites by mass spectrometry. *Biochemistry* 44: 1833–1845, 2005.
151. Wester MR, Johnson EF, Marques-Soares C, Dansette PM, Mansuy D, and Stout CD. Structure of a substrate complex of mammalian cytochrome P450 2C5 at 2.3 Å resolution: Evidence for multiple substrate binding modes. *Biochemistry* 42: 6370–6379, 2003.
152. Wester MR, Johnson EF, Marques-Soares C, Dijols S, Dansette PM, Mansuy D, and Stout CD. Structure of mammalian cytochrome P450 2C5 complexed with diclofenac at 2.1 A resolution: Evidence for an induced fit model of substrate binding. *Biochemistry* 42: 9335–9345, 2003.
153. Wester MR, Yano JK, Schoch GA, Yang C, Griffin KJ, Stout CD, and Johnson EF. The structure of human cytochrome P450 2C9 complexed with flurbiprofen at 2.0-A resolution. *J Biol Chem* 279: 35630-35637, 2004.
154. Whitehouse CJ, Bell SG, Yang W, Yorke JA, Blanford CF, Strong AJ, Morse EJ, Bartlam M, Rao Z, and Wong LL. A highly active single-mutation variant of P450BM3 (CYP102A1). *Chembiochem* 10: 1654–1656, 2009.
155. Williams PA, Cosme J, Sridhar V, Johnson EF, and McRee DE. Mammalian microsomal cytochrome P450 monooxygenase: Structural adaptations for membrane binding and functional diversity. *Mol Cell* 5: 121–131, 2000.
156. Williams PA, Cosme J, Sridhar V, Johnson EF, and McRee DE. Microsomal cytochrome P4502C5: comparison to microbial P450s and unique features. *J Inorg Biochem* 81: 183–190, 2000.
157. Williams PA, Cosme J, Ward A, Angove HC, Matak Vinkovic D, and Jhoti H. Crystal structure of human cytochrome P450 2C9 with bound warfarin. *Nature* 424: 464–468, 2003.
158. Xu LH, Fushinobu S, Ikeda H, Wakagi T, and Shoun H. Crystal structures of cytochrome P450 105P1 from *Streptomyces avermitilis*: Conformational flexibility and histidine ligation state. *J Bacteriol* 191: 1211–1219, 2009.
159. Yano JK, Blasco F, Li H, Schmid RD, Henne A, and Poulos TL. Preliminary characterization and crystal structure of a thermostable cytochrome P450 from *Thermus thermophilus*. *J Biol Chem* 278: 608–616, 2003.
160. Yano JK, Denton TT, Cerny MA, Zhang X, Johnson EF, and Cashman JR. Synthetic inhibitors of cytochrome P450 2A6: Inhibitory activity, difference spectra, mechanism of inhibition, and protein cocrystallization. *J Med Chem* 49: 6987–7001, 2006.
161. Yano JK, Hsu MH, Griffin KJ, Stout CD, and Johnson EF. Structures of human microsomal cytochrome P450 2A6 complexed with coumarin and methoxsalen. *Nat Struct Mol Biol* 12: 822–823, 2005.
162. Yano JK, Koo LS, Schuller DJ, Li H, Ortiz de Montellano PR, and Poulos TL. Crystal structure of a thermophilic cytochrome P450 from the archaeon *Sulfolobus solfataricus*. *J Biol Chem* 275: 31086–31092, 2000.
163. Yano JK, Wester MR, Schoch GA, Griffin KJ, Stout CD, and Johnson EF. The structure of human microsomal cytochrome P450 3A4 determined by X-ray crystallography to 2.05-Å resolution. *J Biol Chem* 279: 38091–38094, 2004.
164. Yao H, McCullough CR, Costache AD, Pullela PK, and Sem DS. Structural evidence for a functionally relevant second camphor binding site in P450cam: Model for substrate entry into a P450 active site. *Proteins-Structure Function Bioinform* 69: 125–138, 2007.
165. Yasutake Y, Imoto N, Fujii Y, Fujii T, Arisawa A, and Tamura T. Crystal structure of cytochrome P450 MoxA from *Nonomuraea recticatena* (CYP105). *Biochem Biophys Res Commun* 361: 876–882, 2007.
166. Yeom H, Sligar SG, Li H, Poulos TL, and Fulco AJ. The role of Thr268 in oxygen activation of cytochrome P450BM-3. *Biochemistry* 34: 14733–14740, 1995.
167. Zerbe K, Pylypenko O, Vitali F, Zhang W, Rouset S, Heck M, Vrijbloed JW, Bischoff D, Bister B, Sussmuth RD, Pelzer S, Wohlleben W, Robinson JA, and Schlichting I. Crystal structure of OxyB, a cytochrome P450 implicated in an oxidative phenol coupling reaction during vancomycin biosynthesis. *J Biol Chem* 277: 47476–47485, 2002.
168. Zhang H, Im SC, and Waskell L. Cytochrome b5 increases the rate of catalysis by cytochrome P4502B4. *Acta Pharmacologica Sinica* 27: 213–213, 2006.
169. Zhang HM, Myshkin E, and Waskell L. Role of cytochrome b(5) in catalysis by cytochrome P4502B4. *Biochem Biophys Res Commun* 338: 499–506, 2005.
170. Zhang W, Pochapsky SS, Pochapsky TC, and Jain NU. Solution NMR structure of putidaredoxin-cytochrome P450cam complex via a combined residual dipolar coupling-spin labeling approach suggests a role for Trp106 of putidaredoxin in complex formation. *J Mol Biol* 384: 349–363, 2008.
171. Zhao B, Guengerich FP, Bellamine A, Lamb DC, Izumikawa M, Lei L, Podust LM, Sundaramoorthy M, Kalaitzis JA, Reddy LM, Kelly SL, Moore BS, Stec D, Voehler M, Falck JR, Shimada T, and Waterman MR. Binding of two flaviolin substrate molecules, oxidative coupling, and crystal structure of *Streptomyces coelicolor* A3(2) cytochrome P450 158A2. *J Biol Chem* 280: 11599–11607, 2005.
172. Zhao B, Guengerich FP, Voehler M, and Waterman MR. Role of active site water molecules and substrate hydroxyl groups in oxygen activation by cytochrome P450 158A2: A new mechanism of proton transfer. *J Biol Chem* 280: 42188–42197, 2005.
173. Zhao B, Lamb DC, Lei L, Kelly SL, Yuan H, Hachey DL, and Waterman MR. Different binding modes of two flaviolin substrate molecules in cytochrome P450 158A1 (CYP158A1) compared to CYP158A2. *Biochemistry* 46: 8725–8733, 2007.
174. Zhao B, Lei L, Vassylyev DG, Lin X, Cane DE, Kelly SL, Yuan H, Lamb DC, and Waterman MR. Crystal structure of albaflavenone monooxygenase containing a moonlighting terpene synthase active site. *J Biol Chem*, 2009.
175. Zhao Y, Sun L, Muralidhara BK, Kumar S, White MA, Stout CD, and Halpert JR. Structural and thermodynamic consequences of 1-(4-chlorophenyl)imidazole binding to cytochrome P450 2B4. *Biochemistry* 46: 11559–11567, 2007.
176. Zhao YH, White MA, Muralidhara BK, Sun L, Halpert JR, and Stout CD. Structure of microsomal cytochrome P4502B4 complexed with the antifungal drug bifonazole. Insight into P450 conformational plasticity and membrane interaction. *J Biol Chem* 281: 5973–5981, 2006.

177. Zhou SF. Drugs behave as substrates, inhibitors and inducers of human cytochrome P450 3A4. *Curr Drug Metab* 9: 310–322, 2008.
178. Zhou SF, Zhou ZW, Yang LP, and Cai JP. Substrates, inducers, inhibitors and structure-activity relationships of human cytochrome P450 2C9 and implications in drug development. *Curr Med Chem* 16: 3480–3675, 2009.
179. Zvelebil M, Wolf CR, and Sternberg MJE. A predicted 3-dimensional structure of human cytochrome. Implications for substrate specificity. *Protein Eng* 4: 271–282, 1991.

Address correspondence to:
Thomas C. Pochapsky
Department of Chemistry
Brandeis University
415 South Street, MS 015
Waltham, MA 02454-9110

E-mail: pochapsk@brandeis.edu

Date of first submission to ARS Central, January 23, 2010; date of final revised submission, March 24, 2010; date of acceptance, May 1, 2010.

Abbreviations Used

Ala = alanine
Arg = arginine
Asn = asparagine
Asp = aspartic acid
CYP = cytochrome P450
Cys = cysteine
Gly = glycine
hϕ = hydrophobic residue
His = histidine
Ile = isoleucines
Leu = leucine
MS = mass spectrometry
NAD(P)H = nicotinamide adenine dinucleotide (phosphate)
NMR = nuclear magnetic resonance
PDB = Protein Data Base (rcsb.org)
Phe = phenylalanine
Pro = proline
Thr = threonine
Trp = tryptophan
Tyr = tyrosine
Val = valine

This article has been cited by:

1. Kiumars Shahrokh, Thomas E. Cheatham, Garold S. Yost. 2012. Conformational dynamics of CYP3A4 demonstrate the important role of Arg212 coupled with the opening of ingress, egress and solvent channels to dehydrogenation of 4-hydroxy-tamoxifen. *Biochimica et Biophysica Acta (BBA) - General Subjects* **1820**:10, 1605-1617. [CrossRef]
2. Renata A. Kwiecie#, Jean-Yves Le Questel, Jacques Lebreton, Marcel Delaforge, François André, Emilie Pihan, Anaïs Roussel, Anaïs Fournial, Piotr Paneth, Richard J. Robins. 2012. Cytochrome P450-Catalyzed Degradation of Nicotine: Fundamental Parameters Determining Hydroxylation by Cytochrome P450 2A6 at the 5#-Carbon or the N -Methyl Carbon. *The Journal of Physical Chemistry B* **116**:27, 7827-7840. [CrossRef]
3. Michael Piazza, Kathryn Futrega, Donald E. Spratt, Thorsten Dieckmann, J. Guy Guillemette. 2012. Structure and Dynamics of Calmodulin (CaM) Bound to Nitric Oxide Synthase Peptides: Effects of a Phosphomimetic CaM Mutation. *Biochemistry* 120416160024001. [CrossRef]
4. Eliana K. Asciutto, Matthew J. Young, Jeffry Madura, Susan Sondej Pochapsky, Thomas C. Pochapsky. 2012. Solution Structural Ensembles of Substrate-Free Cytochrome P450 cam. *Biochemistry* 120410101221007. [CrossRef]
5. Rudi Fasan. 2012. Tuning P450 Enzymes as Oxidation Catalysts. *ACS Catalysis* 647-666. [CrossRef]
6. Stephen G. Bell, Wen Yang, Jake A. Yorke, Weihong Zhou, Hui Wang, Jeffrey Harmer, Rachel Copley, Aili Zhang, Ruimin Zhou, Mark Bartlam, Zihe Rao, Luet-Lok Wong. 2012. Structure and function of CYP108D1 from Novosphingobium aromaticivorans DSM12444: an aromatic hydrocarbon-binding P450 enzyme. *Acta Crystallographica Section D Biological Crystallography* **68**:3, 277-291. [CrossRef]
7. M. Kokkinidis, N.M. Glykos, V.E. FadouloglouProtein Flexibility and Enzymatic Catalysis **87**, 181-218. [CrossRef]
8. Stephen G. Bell, Wen Yang, Adrian B. H. Tan, Ruimin Zhou, Eachan O. D. Johnson, Aili Zhang, Weihong Zhou, Zihe Rao, Luet-Lok Wong. 2012. The crystal structures of 4-methoxybenzoate bound CYP199A2 and CYP199A4: structural changes on substrate binding and the identification of an anion binding site. *Dalton Transactions* **41**:28, 8703. [CrossRef]
9. Larissa M. Podust, David H. Sherman. 2012. Diversity of P450 enzymes in the biosynthesis of natural products. *Natural Product Reports* **29**:10, 1251. [CrossRef]
10. V.B. Urlacher7.13 Oxidation: Stereoselective Oxidations with Cytochrome P450 Monooxygenases 275-294. [CrossRef]
11. Hongmao Sun, Henrike Veith, Menghang Xia, Christopher P. Austin, Ruili Huang. 2011. Predictive Models for Cytochrome P450 Isozymes Based on Quantitative High Throughput Screening Data. *Journal of Chemical Information and Modeling* 110926154521006. [CrossRef]
12. Øyvind L. Busk, Doreen Ndossi, Steven Verhaegen, Lisa Connolly, Gunnar Eriksen, Erik Ropstad, Morten Sørlie. 2011. Relative quantification of the proteomic changes associated with the mycotoxin zearalenone in the H295R steroidogenesis model. *Toxicon* . [CrossRef]
13. Karel Berka, Tereza Hendrychova#, Pavel Anzenbacher, Michal Otyepka. 2011. Membrane Position of Ibuprofen Agrees with Suggested Access Path Entrance to Cytochrome P450 2C9 Active Site. *The Journal of Physical Chemistry A* 110711170921004. [CrossRef]
14. Sang Taek Jung, Ryan Lauchli, Frances H Arnold. 2011. Cytochrome P450: taming a wild type enzyme. *Current Opinion in Biotechnology* . [CrossRef]
15. Abhinav Luthra, Ilia G. Denisov, Stephen G. Sligar. 2011. Spectroscopic features of cytochrome P450 reaction intermediates. *Archives of Biochemistry and Biophysics* **507**:1, 26-35. [CrossRef]
16. Marina Dang, Susan Sondej Pochapsky, Thomas C. Pochapsky. 2011. Spring-loading the active site of cytochrome P450cam. *Metallomics* **3**:4, 339. [CrossRef]